

AN ALL-OPTICAL EXCITONIC SWITCH TEMPLATED ON A DNA SCAFFOLD  
OPERATED IN THE LIQUID AND SOLID PHASES

by

Donald L. Kellis



A thesis

submitted in partial fulfillment

of the requirements for the degree of

Master of Science in Materials Science and Engineering

Boise State University

May 2020

© 2020

Donald L. Kellis

**ALL RIGHTS RESERVED**

BOISE STATE UNIVERSITY GRADUATE COLLEGE

**DEFENSE COMMITTEE AND FINAL READING APPROVALS**

of the thesis submitted by

Donald L. Kellis

Thesis Title: An All-Optical Excitonic Switch Templated on a DNA Scaffold Operated  
in the Liquid and Solid Phases

Date of Final Oral Examination: 6 March 2020

The following individuals read and discussed the thesis submitted by student Donald L. Kellis, and they evaluated their presentation and response to questions during the final oral examination. They found that the student passed the final oral examination.

William B. Knowlton, Ph.D. Co-Chair, Supervisory Committee

Bernard Yurke, Ph.D. Co-Chair, Supervisory Committee

Andres Jäschke, Ph.D. Member, Supervisory Committee

The final reading approval of the thesis was granted by William B. Knowlton, Ph.D., Co-Chair of the Supervisory Committee. The thesis was approved by the Graduate College.

## DEDICATION

This thesis is dedicated to my family without whom my journey would not have been possible. The trials and tribulations you have all encountered, embraced, and walked through continues to provide insight and inspiration to me, I love you all.

## ACKNOWLEDGMENTS

I would like to acknowledge and thank my advisor(s), Drs. William B. Knowlton, Bernard Yurke, and Andres Jäschke. Your tireless support and encouragement have provided me opportunities, freedom, and insight to overcome any obstacles I encountered along the way. I owe a debt of gratitude to professor Billy Hudson without whom I would have never worked through my fear and apprehension of mathematics, your guidance and continued conversations have lifted my soul throughout my academic journey. I express my deepest appreciation to my colleagues of the Nanoscale Materials & Device Group here at Boise State University, your contributions, insights, discussions, and inspiration have shown me just how important teamwork and outreach are to achieving ones goals.

## ABSTRACT

The natural excitonic circuitry of photosynthetic organisms, including light harvesting antennas, provides a distinctive example of a highly attractive bio-inspired alternative to electronic circuits. Excitonics, which capitalizes on spatially arranged optically active molecules ability to capture and transfer light energy below the diffraction limit of light has garnered recognition as a potential disruptive replacement for electronic circuits. However, assembly of optically active molecules to construct even simple excitonic devices has been impeded by the limited maturity of suitable molecular scale assembly technologies.

An example of nanophotonic circuitry, natural light harvesting antennas employ proteins as scaffolds to organize and self-assemble light-active molecules into excitonic networks capable of capturing and converting light to excitonic energy, and transferring that energy at ambient temperature. Protein self-assembly is extremely complex due to the over 20 amino acids building blocks used in the self-assembly process and the difficulty of predicting how proteins actually fold. An alternative method for organization and self-assembly may be found in the field DNA nanotechnology.

DNA nanotechnology provides the most viable means to organize optically active molecules as there are only four nucleic acid building blocks and well-established simple design rules. Leveraging DNA nanotechnology will meet the requirements of precise proximity (selectivity) and appropriate number (specificity) needed to create larger arrays of multifunctional optically active molecules. Employing the design rules of DNA self-

assembly, we have designed, engineered and operated an all-optical excitonic switch consisting of donor and acceptor chromophores and diarylethene photochromic modulating units assembled with nanometer scale precision.

This work demonstrates the first integration of three diarylethene photochromic units into a single DNA oligonucleotide. Photoisomerization of diarylethenes has been shown to be one of the fastest photochemical reactions thereby affording potential switching speeds in the 10's of picoseconds. Adopting diarylethenes as optically reversible switching units provided the ability to operate the all-optical excitonic switch through nearly 200 cycles without overt cyclic fatigue and excellent ON/OFF stability in both the liquid and solid phases.

Assessing the static and dynamic cycling behavior of the all-optical excitonic switch allowed for the development of a model to predict characteristic switching times ( $\tau$ ) of 17.0 and 23.3 seconds for the liquid and solid phases, respectively which align well with the experimental data thereby validating the model. While these times are much faster than that of other non-optically based DNA-templated excitonic switches ( $\tau \sim 10$ 's of minutes), the times noted here are limited by the steady-state optical instrumentation, (i.e., photon flux, detector integration time, and slit cycling speed), used to characterize the all-optical excitonic switches. Our model predicts switching times in the picosecond range could be achieved with the use of a high peak power ultrafast laser. First-order calculations estimate the all-optical excitonic switch has a footprint 37X smaller, a smaller volume by over 3 orders of magnitude and over an order of magnitude less energy per cycle than a state-of-the-art MOSFET.

These findings, combined with no production of waste products and the potential ability to switch at speeds in the 10's of picoseconds, establishes a prospective pathway toward all-optical excitonic circuits.



## TABLE OF CONTENTS

DEDICATION .....	iv
ACKNOWLEDGMENTS .....	v
ABSTRACT.....	vi
LIST OF TABLES .....	xii
LIST OF FIGURES .....	xiii
LIST OF ABBREVIATIONS.....	xvii
LIST OF SYMBOLS .....	xxii
CHAPTER ONE: INTRODUCTION.....	1
References.....	6
CHAPTER TWO: AN ALL-OPTICAL EXCITONIC SWITCH OPERATED IN THE LIQUID AND SOLID PHASES .....	9
Abstract.....	11
2.1 Introduction.....	11
2.2 Results and Discussion .....	14
2.2.1 Design .....	14
2.3 Excitonic Modulation.....	19
2.4 Characteristic Switching Times .....	21
2.5 Cyclic Fatigue Assessment .....	25
2.6 Methods.....	26
2.6.1 Photochromic Nucleotide Synthesis .....	26

2.6.2 Solid Phase Synthesis of Modified Oligonucleotides .....	27
2.6.3 HPLC Purification .....	28
2.6.4 LC/MS Analysis.....	28
2.6.5 Single Stranded DNA (ssDNA) Sequence Design .....	29
2.6.6 Spectral Overlap Design .....	29
2.6.7 All-optical Switch Hybridization.....	30
2.6.8 Fluorescence Measurements.....	30
2.6.9 Dynamic Modulation Measurements.....	31
2.7 Conclusion .....	31
2.8 Author Justifications .....	32
2.9 Acknowledgements.....	34
References.....	34
3.0 Supporting Information.....	39
3.1 Switching contrast, cyclic fatigue, cycle time, modulation, and photostability.....	39
3.2 Synthesis of the phosphoramidite for solid phase synthesis.....	39
3.3 Normalized and unaltered spectral overlap data and chromophore selection .....	41
3.4 Determination of the switching efficiency of PS1 (quantitative composition of the photostationary state).....	43
3.5 Absorbance of one <i>versus</i> three photochromic nucleotides.....	45
3.6 Fluorescence measurements.....	47
3.7 Controls.....	48
3.8 Solid phase concentration calculations .....	50
3.9 Solid phase variation.....	55

3.10 Switching time derivation: .....	55
3.11 Characteristic switching time derivation .....	57
3.12 Time trial design .....	62
3.13 Absorbance cross section .....	63
3.14 Photon energy, photon fluence, and photon flux .....	64
3.15 Ultrafast laser switching .....	65
3.16 Comparison of the all-optical excitonic switch to a 14 nm node FinFET .....	66
3.17 Photochromic nucleotide synthesis, attachment, and purification.....	71
References .....	78
CHAPTER THREE: SUMMARY AND FUTURE WORK .....	80

## LIST OF TABLES

Table 3.1	Single strand DNA sequences.....	40
Table 3.2	HPLC gradient for the determination of the switching efficiency of PS1	44
Table 3.3	Liquid and solid phase concentration values .....	55
Table 3.4	Summed exposure times ( $\tau\Sigma$ ) for time trial experiments conducted with the all-optical excitonic switch. One complete cycle ( $t_o + t_c$ ) is given as $\tau\Sigma$ and the average time of all values with the standard deviations are included.....	63
Table 3.5	Bulk Low Power 14 nm technology node FinFET parameters (after6)....	68
Table 3.6	Parameters for All-Optical Excitonic Switch .....	69
Table 3.7	Nucleotide modification.....	76
Table 3.8	Mass, sequence and chemical formula of the synthesized oligonucleotides. ....	76
Table 3.9	Gradients for preparative HPLC purification of the synthesized oligonucleotides .....	76
Table 3.10	HPLC gradient for LC/MS measurements.....	77

## LIST OF FIGURES

- Figure 1.1 Number of successful cycles of the all-optical excitonic switch as compared to other DNA-templated excitonic switches (refs. 17, 20, 21, 30). The other switches must all be in liquid solution to operate and show cyclic fatigue within the first 10 cycles (see inset). In contrast, our switch operates in both the liquid and solid phase with no apparent cyclic fatigue, and could have easily been cycled beyond the 199 cycles shown. Although time is not included here, the cycle time for references 2-4 is about 40 minutes, roughly 2 minutes for reference 1, and 1 minute for our data shown here (although we have demonstrated 10 second cycle times)..... 4
- Figure 2.1 All-optical excitonic switch design. (a, b) Schematic of the all-optical excitonic switch with one and three photochromic nucleotides, respectively. (c) Schematic of the self-assembly process allowing for precisely controlled placement of the optical components employed in the all-optical excitonic switch through binding domains. (d) Normalized absorption spectra of the photochromic strands in the CLOSED (absorbing) and OPEN (non-absorbing) configurations. Schematic insets illustrate molecular configuration changes occurring in the photochromic nucleotides with the ring system formed or opened highlighted in red. (e, f) Normalized absorption and emission spectra of the donor and acceptor strands, respectively, utilized in this study. (g) Relative absorbance spectra of photochromic strands containing a single photochromic nucleotide (design scheme 1a) versus three photochromic nucleotides (design scheme 1b), illustrating the three-fold increase in absorption (Supporting Information S5 and Figure S3). (h) Static emission plots of the all-optical excitonic switch in the ON and OFF state collected using the two design schemes (1a & 1b) from this study. Of note is the increased difference between the ON state and OFF state when the triple photochromic strand (lower plot) is employed, indicating improved excitonic modulation with design scheme 1b. .... 18
- Figure 2.2 All-optical excitonic switch emission. Emission modulation data for the all-optical excitonic switch with three photochromic nucleotides attached (as illustrated in Figure 1b) operated at concentrations of 20  $\mu\text{M}$  in the liquid (a-c) and 52 mM (calculated) in the solid (Supporting Information S8, Figure S6, and Table S3) (d-f) phases with an exposure time of 30 seconds. (a & d) Static emission plots of the all-optical excitonic switch in the ON and OFF states demonstrating modulation between the donor and the acceptor emission maxima. A blue shift in the solid phase donor

emission is noted (Supporting Information S9). (b & e) Saw-tooth plots demonstrating the changes in the donor and acceptor emission as the photochromic nucleotides are cycled between the open (O) and closed (C) configuration (i.e. ON and OFF states) six times, with near complete resetting of the all-optical excitonic switch between each cycle (i.e., no evidence of cyclic fatigue). Dashed lines have been added to aid in visualizing an ON/OFF threshold between the open and closed configuration of the photochromic nucleotide for both the donor and acceptor emission. (c & f) Dynamic modulation emission plots of the donor and the acceptor strand as the photochromic nucleotides are cycled between the open and the closed configuration six times; exponential behavior indicates first-order reaction kinetics. .... 21

Figure 2.3 Characteristic all-optical excitonic switch time. Characteristic switching time ( $t_s$ ) determination from the liquid and solid phase time trial experiments (a & d). Representative averaged saw-tooth plots extracted from 30 second exposure time liquid and solid phase time trial static emission scans (b & e). Representative dynamic modulation plots of the donor and acceptor emission by the photochromic nucleotides with exponential decay fits, extracted  $\tau_c$ ,  $\tau_o$ , &  $\tau_\Sigma$  times given (c & f). Switching amplitude ( $\Delta_s$ ) versus photochromic nucleotide exposure time ( $t_e$ ) of the photochromic nucleotides plotted with the first order reaction kinetics model (Eq. 9 Supporting Information S10). Error bars were generated from averaged standard deviations of each time trial  $\Delta_s$  series. .... 24

Figure 2.4 Cyclic fatigue assessment. Cycling of the all-optical excitonic switch operated at a concentration of 20  $\mu\text{M}$  in the liquid (a), and 52 mM in the solid (b) phases with an exposure time of 30 seconds performed nearly 200 times over the course of 100 minutes. Dynamic modulation scans were performed by exposing the photochromic nucleotides with ultraviolet (UV)  $\lambda_{\text{exc}}\text{ON} \rightarrow \text{OFF } 300\text{nm}$  or visible (VIS)  $\lambda_{\text{exc}}\text{OFF} \rightarrow \text{ON } 455\text{nm}$  light while monitoring the acceptor emission at 520 nm. Saw-tooth plots were created by averaging the final ten seconds of each cycling event to produce a single data point. About 6% or 5% random variation over the entire cycling range was determined for both the ON and OFF states in the liquid and the solid, respectively. Insets show that little cycle to cycle variation is observed, with values of both variation and  $\Delta_s$  exhibiting little change. No apparent cyclic fatigue is observed over the course of the trial within the resolution of the experiment. .... 26

Scheme 3.1 Reaction pathway to synthesize the photoswitchable phosphoramidite building block (3) needed for solid phase synthesis. .... 39

Figure 3.1 Spectral overlap of the optical components comprising the all-optical excitonic switch. (a) Shown are the normalized absorption and emission

spectra of the donor strand (blue dashed and solid curves, respectively), normalized absorption spectra of the photochromic nucleotides in both the open (non-absorbing, red dashed/dotted curve) and closed (absorbing, red dashed curve) configurations, and normalized absorption and emission spectra of the acceptor strand (green dashed and solid curves, respectively). Optical molecules were selected such that overlap occurred among the donor emission, photochromic nucleotide closed configuration absorption, and acceptor absorption in order to modulate both the excitonic transfer and FRET processes. Exposure wavelengths were chosen such that minimal perturbation to the configuration of the photochromic nucleotides would occur during data collection. Up arrows indicate the wavelengths used to expose the optical molecule and the down arrow indicates the wavelength used to collect spectral data. The spectra have been normalized in order to easily visualize the spectral overlap in the 350-550 nm region. (b) The actual unaltered absorbance of the acceptor as well as the three photochromic nucleotides in their open and closed states. A comparison of the spectra highlights that the absorbance of the three photochromic nucleotides at the donor emission maximum ( $\lambda_{\text{max}} = 460 \text{ nm}$ ) is approximately 6x lower the acceptor. The vertical double-headed arrow indicates the donor's peak emission wavelength of 460 nm..... 42

Figure 3.2 HPLC time trace of PS1 after 10 min of UV-irradiation with a 310 nm LED (Thorlabs M310L3) at 260 nm..... 44

Figure 3.2 Saw-tooth plots of the all-optical excitonic switch operating in the liquid phase demonstrating the changes in the donor and acceptor emission as the photochromic nucleotides are cycled between the open and closed configuration (i.e., ON and OFF states) six times. (a) 5 $\mu\text{M}$  switch with a single photochromic nucleotide (strand PS1) demonstrates minimal modulation between the ON and OFF states. (b) 20 $\mu\text{M}$  switch with a PS1 strand demonstrates 6.6% modulation between the ON and OFF state. The weak modulation noted in a may be due to the emission of the donor/acceptor pair overwhelming the single photochromic nucleotide as well as the low absorbance of the single photochromic nucleotide. (c) 5 $\mu\text{M}$  switch with three photochromic nucleotides attached (PS3 strand) demonstrates 8.2% modulation between the ON and OFF states. (d) 20 $\mu\text{M}$  switch with a PS3 strand produces the greatest amount of donor/acceptor emission modulation (15.1%). The increased modulation results from the greater absorbance provided by the three photochromic nucleotides. .... 46

Figure 3.3 Detector geometry for acquisition of all-optical excitonic emission spectra. For the liquid environment measurements, a perpendicular excitation light source interacts with the sample via a 2 mm by 2 mm window on the source side of the cuvette. The fluorescence emission is transmitted through a 2 mm by 10 mm window on the detector side of the cuvette

(cyan lines) and detected via a photomultiplier tube (PMT, detector) aligned at 90° relative to the excitation. For the solid environment measurements, the excitation light source remained perpendicular to the sample, but the detector samples fluorescence emission aligned ~180° relative to the sample (purple lines). The solid alignment geometry is required because very little fluorescence emission is delivered in the direction parallel to the quartz slide..... 47

Figure 3.4 All-optical excitonic switch controls performed at 5 μM DNA concentration in the liquid environment. (a, b, c) Donor with three photochromic nucleotides hybridized (no acceptor present) produced slight modulation of the donor emission, indicating excitonic absorption and FRET transfer interruption. (d, e, f) Acceptor with three photochromic molecules hybridized (no donor present) produced slight acceptor emission modulation demonstrating excitonic absorption and FRET transfer interruption. (g, h, i) Donor/Acceptor with no photochromic nucleotides hybridized produced no significant modulation of either the donor or acceptor emission curve, signifying the excitonic absorption and FRET transfer interruption is directly attributable to the presence of the photochromic nucleotides. (j, k, l) Donor/Acceptor dyes hybridized plus three photochromic nucleotides hybridized to a bare all-excitonic construct outside the Förster radius produced negligible modulation. All data presented without normalization for concentration nor (in the case of k, l) for dilution. .... 50

Figure 3.5 (a) Representative solid phase sample imaged using a 534 nm excitation filter and a 606 nm emission filter; the grayscale image was reversed for clarity. A clear elliptical ring on the outer periphery can be observed in the image indicating the all-optical excitonic switch migrates to the edges of the sample during desiccation. The elliptical ring dimensions are confined within the window size of the fluorometer excitation beam. (b) 3D profilometer map of a representative solid phase sample where the elliptical ring is observed within the outer periphery of the sample. (c & d) Profilometer data collected from the solid phase sample along the lateral and longitudinal directions of the ellipse. For each direction, the sample height and the inner and outer ellipse radii are indicated. Note that the profiles have been divided into the non-fluorescing region (light shading) and the fluorescing region (dark shading). .... 54

Figure 3.6 HPLC chromatograms of the synthesized oligonucleotides with one modification (PS1) and three modifications (PS3), detected at 280 nm... 77



## LIST OF ABBREVIATIONS

$J_{app}$	Apparent coupling constant
aJ	Attojoule
$A_i$	Area of the inner elliptical ring
$A_e$	Area of the entire elliptical ring
$A_r$	Area of the outer elliptical ring
$N_A$	Avogadro's number
$C_r$	Concentration in the outer elliptical ring
$C_{liq}$	Concentration of the liquid
CPU	Computer processing unit
CPG	Controlled pore glass
$^{\circ}C$	Degrees Celsius
DAD	Diode array detector
DNA	Deoxyribonucleic acid
dsDNA	Double strand deoxyribonucleic acid
dU	Deoxyuridine
$EOT$	Effective oxide thickness
$I_{closed}$	Emission intensity closed configuration
$I_{offset}$	Emission intensity offset
$I_{open}$	Emission intensity open configuration

EDTA	Ethylenediaminetetraacetic acid
$t_e$	Exposure time
$t_{(1/2)}$	Exposure time to cycle half the photochromic nucleotides
$H_{FO}$	Field oxide height
FinFET	Fin field-effect transistor
$H_F$	Fin height
$W_{fin}$	Fin width
$I$	Final emission intensity
FRET	Förster resonance energy transfer
$L_g$	Gate length
HfO <sub>2</sub>	Hafnium dioxide
$H_r$	Height of the outer elliptical ring
Hz	Hertz
$k_{ox}$	High-k dielectric constant of the oxide
$t_{HK}$	High-k dielectric thickness
$k_{HK}$	High-k relative dielectric constant
HPLC	High-performance liquid chromatography
pH	Hydrogen ion activity
$I_0$	Initial emission intensity
$t_{IL}$	Interfacial oxide layer thickness
$k_{IL}$	Interfacial oxide relative dielectric constant
$C_{inv}$	Inversion capacitance

kHz	Kilohertz
$I_{leak}$	Leakage current
$l$	Length
LED	Light emitting diode
L	Liter
LC-MS	Liquid chromatography / mass spectrum
$C_{load}$	Load capacitance
MOSFET	Metal-oxide-semiconductor field-effect transistor
m	Meter
$\mu\text{J}$	Microjoule
$\mu\text{M}$	Micromolar
mL	Milliliter
mm	Millimeter
mM	Millimolar
nm	Nanometer
NMR	Nuclear magnetic resonance
NUPACK	Nucleic acid package
$f$	Operation frequency
OD	Optical density
OPA	Optical parametric amplifier
ppm	Parts per million
pcFRET	Photochromic Förster resonance energy transfer

$E$	Photon energy
$H$	Photon fluence
$J$	Photon flux
$I_c$	Photon flux to close the photochromic nucleotide
$I_o$	Photon flux to open the photochromic nucleotide
$h$	Planck's constant
PAGE	Polyacrylamide gel electrophoresis
$W$	Power
$P$	Probability of photochromic nucleotide switching
$t_Q$	Quantum mechanical inversion layer thickness
$r$	Radius
s	Second
PS1	Single photochromic nucleotide strand
$c$	Speed of light
$A$	Spot size area
SOTA	State-of-the-art
$V_{dd}$	Supply voltage
$t_s$	Switching time
TMS	Tetramethylsilane
TLC	Thin film chromatography
3D	Three dimensional
PS3	Three photochromic nucleotide strand

TAE	Tris(hydroxymethyl)aminomethane
UHP	Ultra-high purity
UV	Ultraviolet
VIS	Visible
$V_{dsDNA}$	Volume of the double stranded DNA scaffold
$V_{liq}$	Volume of the liquid
$V_r$	Volume of the outer elliptical ring

## LIST OF SYMBOLS

$\sigma$	Absorbance cross-section
$\sigma_c$	Absorbance cross-sectional area closed photochromic nucleotides
$\sigma_o$	Absorbance cross-sectional area open photochromic nucleotides
$\text{\AA}$	Angstrom
$\delta$	Chemical shifts
$[C]$	Concentration of closed photochromic nucleotides
$[O]$	Concentration of open photochromic nucleotides
$\lambda_{em}$	Emission wavelength
$\lambda_{ex}$	Excitation wavelength
$\lambda_{ex}^{OFF \rightarrow ON}$	Excitation wavelength to cycle from open configuration to the closed configuration
$\lambda_{ex}^{ON \rightarrow OFF}$	Excitation wavelength to cycle from closed configuration to the open configuration
$\tau_i$	Mean time for modulation
$\tau_c$	Mean time to close
$\tau_o$	Mean time to open
$\mathcal{E}_o$	Permittivity of free space
$\pi$	Pi
$\tau_\Sigma$	Sum of the mean time to open and mean time to close
$\gamma_i$	Switching rate

$\gamma_c$	Switching rate to close
$\gamma_o$	Switching rate to open
$\lambda$	Wavelength

## CHAPTER ONE: INTRODUCTION

This thesis is based on “An All-Optical Excitonic Switch Operated in the Liquid and Solid Phases” published in ACS Nano (Chapter Two, published).

Recently, the Semiconductor Industry Association (SIA) has announced the imminent end of feature scaling based on Moore’s Law<sup>1-2</sup> which amplifies the need for alternative technological approaches to supplant current complimentary metal-oxide-semiconductor (CMOS) circuit fabrication methods. Convergence of current semiconductor fabrication techniques with biological inspiration offers a pathway for disruptive new designs and processes as outlined under five SIA roadmaps<sup>1</sup>.

Drawing motivation from nature<sup>3</sup>, photosynthetic organisms ability to capture and convert sunlight to excitonic energy with subsequent rapid excitonic energy transfer offers a distinctive example of natural nanophotonic circuitry<sup>4</sup> as a highly attractive substitute to electronic circuits. Through trial and error, nature has optimized the folding of proteins to self-assemble molecular breadboards to organize optically active molecules (i.e., chromophores) creating highly effective nanophotonic circuits that operate at ambient temperatures.

Nanophotonics, including plasmonics and excitonics, has received considerable attention as an alternative technology for electronic circuitry<sup>5</sup>. The ultimate goal of nanophotonics is to control the interaction of light and matter in a predictable manner. Excitonics in particular exploits chromophores to capture and transport light energy below the diffraction limit of light.



Leveraging the capture and transport of light energy as well as the packing density possible with chromophores, optical devices using only excitons in their operation presents a tantalizing method for overcoming feature size limitations currently facing the semiconductor industry.

A crucial question concerning building viable nanophotonic circuits involves the ability to selectively place small optically active components with precision and control. While photosynthetic organisms have nearly perfected nanophotonic circuitry through protein self-assembly and chromophore organization, the self-assembly of proteins is very complicated owing to over 20 amino acid building blocks which is then compounded by the difficulty of successfully folding amino acids into predictable structures. A much simpler method of creating self-assembled molecular breadboards can be realized using deoxyribose nucleic acid (DNA) nanotechnology. Pioneered by the likes of Seeman<sup>6</sup>, Rothmund<sup>7</sup>, Douglas<sup>8</sup>, and others, DNA nanotechnology provides rapid prototyping<sup>9-10</sup> and elegant control over the creation of 1D, 2D, and 3D structures with only four nucleic acid building blocks and well-established design rules<sup>11</sup>. The bottom-up approach employed by DNA nanotechnology provides a far smaller size scale than current top-down methods which are reaching their scaling limits.

Covalent attachment of chromophores to DNA has blossomed over the years allowing for precise positioning and arrangement of over 200 different chromophores<sup>12-15</sup> within synthetic DNA strands. The large catalog of chromophores opens the possibility for successful design and production of excitonic devices, however the majority exploit Förster resonance energy transfer (FRET).

FRET cascades<sup>16</sup>, energy ratchet<sup>17-18</sup>, logic gates<sup>19-20</sup>, and switch<sup>21-22</sup> devices have been assembled using DNA scaffold templates. The bulk of these devices implement DNA strand displacement, pioneered by Yurke et al.<sup>23</sup>, to disrupt the FRET process thereby inducing excitonic modulation, or switching, initiating the field of dynamic DNA nanotechnology<sup>24</sup>. The strand displacement process requires the dissociation and hybridization of double stranded DNA (dsDNA) which can take 20 minutes or more to occur and must be performed in an aqueous environment. The time and environment constraints of excitonic switching via strand displacement may be useful in colorimetric detection schemes for medical or genetic purposes; however, it is not practical as a viable alternative to supplant current complimentary metal-oxide-semiconductor (CMOS) devices or circuitry.

Ideally, an excitonic switch that can compete with CMOS devices must be able to interrupt or modulate the FRET process quickly ( $>10$  ps)<sup>25</sup> and efficiently (i.e., energy per cycle  $>10$  aJ)<sup>26</sup>. Challenges to construct technologically relevant excitonic circuits include: (i) achieving devices capable of employing only excitons in their operation, (ii) developing scalable networks suitable for distributing small chromophores, (iii) selectively placing specific numbers of chromophores on networks in a variety of configurations with precision and control, and (iv) identifying chromophores which may be discretely addressed by markedly different wavelengths of light.

Current methods being explored for operation of DNA scaffolded FRET-based switches include chromophore mediation<sup>27-28</sup>, chromophore quenching<sup>28-30</sup>, and intercalation of optically active molecules<sup>31-32</sup>. While activating and deactivating DNA templated chromophores optically or through chemical changes has led to improved

switching times over DNA strand displacement, deactivation requires up to 10 minutes producing noticeable degradation (i.e., cyclic fatigue) between the On-state and the Off-state within a few switching cycling events as shown in figure 1 (i.e., Kellis et al.<sup>17</sup>, Cannon et al.<sup>20</sup>, Graugnard et al.<sup>21</sup>, Laboda et al.<sup>30</sup>). Hence, designing and operating an all-optical excitonic switch capable of cycle times in the picosecond regime, with means of controlling the selectivity and specificity of the optical components on scalable DNA templates while limiting cyclic fatigue, emissive degradation without the need for dissociation in both liquid and solid phase, remains elusive.

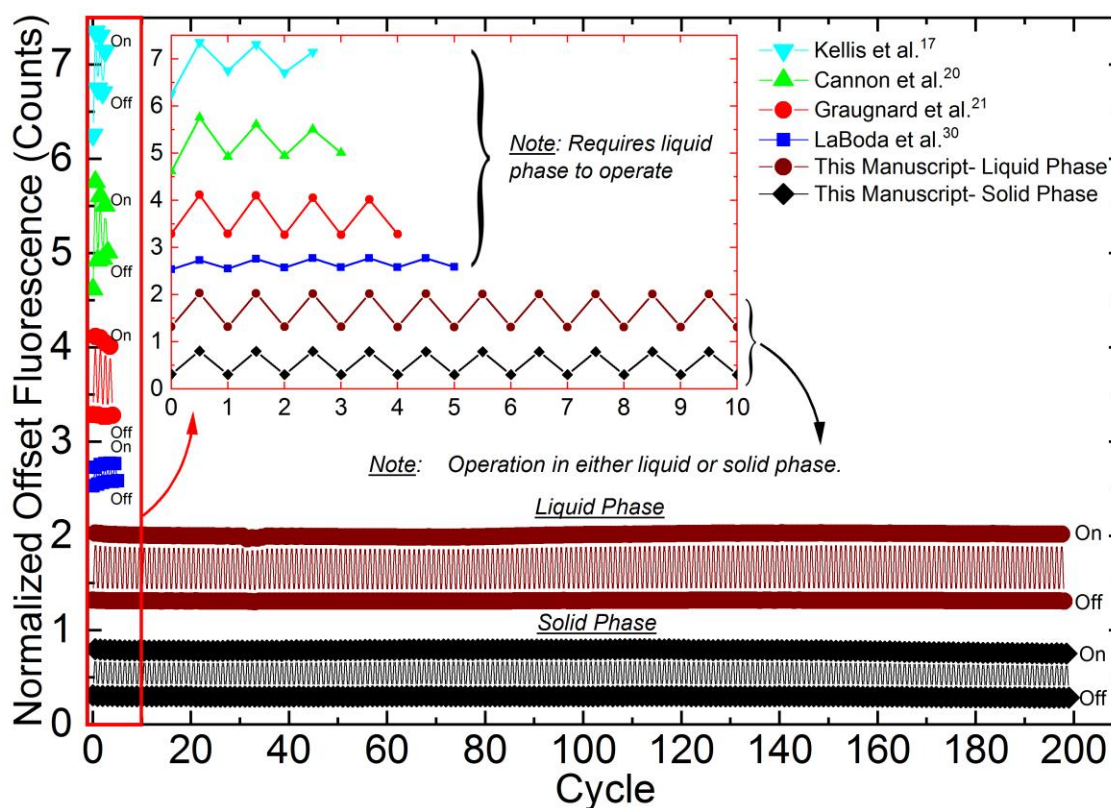


**Figure 1.1** Number of successful cycles of the all-optical excitonic switch as compared to other DNA-templated excitonic switches (refs. 17, 20, 21, 30). The other switches must all be in liquid solution to operate and show cyclic fatigue within the first 10 cycles (see inset). In contrast, our switch operates in both the liquid and solid phase with no apparent cyclic fatigue, and could have easily been cycled beyond the 199 cycles shown. Although time is not included here, the cycle time for references 2-4 is about 40 minutes, roughly 2 minutes for reference 1, and 1 minute for our data shown here (although we have demonstrated 10 second cycle times).

All-optical excitonic switches have been demonstrated using photochromic molecules to modulate covalently attached donors in a process termed photochromic Förster resonance energy transfer (pcFRET), however, doing so on scalable templates has yet to be achieved. Addressing the challenges of feature scaling, controlled design, excitonic energy transfer, and molecular organization, we fabricated an all-optical excitonic switch employing photochromic units in both the liquid and solid phase. We demonstrate both selectivity and specificity using DNA scaffolded self-assembly that is over two orders of magnitude faster than strand displacement and intercalation, 6 times faster than DNA scaffolded chromophore quenching, and 5 times faster than pcFRET switches. Simple calculations indicate a footprint, volume, and energy consumption equal to or better than some of today's state-of-the-art low power metal oxide semiconductor field effect transistors (MOSFETs).

This thesis is presented in three chapters the bulk of which is composed of a published paper<sup>33</sup>. Chapter 2 provides an introduction to the design requirements for successful all-optical excitonic switching employing a DNA scaffolded template. This chapter specifically details the resulting work which demonstrates an all-optical excitonic switch that can be operated in both the liquid and the solid phase without noticeable degradation. Chapter 3 discusses key aspects and potential directions for continued work with all-optical excitonic switches.

## References

1. Semiconductor Industry Association, *Rebooting the IT Revolution*, **2015**.
2. Waldrop, M. M., The chips are down for Moore's law. *Nature News* **2016**, 530 (7589), 144.
3. Scholes, G. D.; Fleming, G. R.; Olaya-Castro, A.; Van Grondelle, R., Lessons from nature about solar light harvesting. *Nature chemistry* **2011**, 3 (10), 763.
4. Scholes, G. D., Quantum biology: coherence in photosynthesis. *Nature Physics* **2011**, 7 (6), 448.
5. Kuzyk, A.; Jungmann, R.; Acuna, G. P.; Liu, N., DNA Origami Route for Nanophotonics. *ACS Photonics* **2018**, 5 (4), 1151-1163.
6. Seeman, N. C.; Kallenbach, N. R., Design of immobile nucleic acid junctions. *Biophysical journal* **1983**, 44 (2), 201-209.
7. Rothmund, P. W. K., Folding DNA to create nanoscale shapes and patterns. *Nature* **2006**, 440 (7082), 297.
8. Douglas, S. M.; Dietz, H., *et al.*, Self-assembly of DNA into nanoscale three-dimensional shapes. *Nature* **2009**, 459 (7245), 414.
9. Ke, Y.; Ong, L. L.; Shih, W. M.; Yin, P., Three-dimensional structures self-assembled from DNA bricks. *science* **2012**, 338 (6111), 1177-1183.
10. Wei, B.; Dai, M.; Yin, P., Complex shapes self-assembled from single-stranded DNA tiles. *Nature* **2012**, 485 (7400), 623-626.
11. Chidchob, P.; Sleiman, H. F., Recent advances in DNA nanotechnology. *Current Opinion in Chemical Biology* **2018**, 46, 63-70.
12. Biosynthesis, Fluorescent Labeled Oligos. <https://www.biosyn.com/fluorescent-labeled-oligos.aspx> (accessed June 12, 2018).
13. Dyomics, Products. <https://dyomics.com/en/products.html> (accessed November 26, 2019).
14. IDT DNA, Dyes. <https://www.idtdna.com/site/Catalog/Modifications/Dyes> (accessed November 18, 2019).
15. Lumiprobe, Fluorophore Chart. <https://www.lumiprobe.com/fluorophore-chart> (accessed December 12, 2019).

16. Bui, H.; Díaz, S. A., *et al.*, Utilizing the Organizational Power of DNA Scaffolds for New Nanophotonic Applications. *Advanced Optical Materials* **2019**, *7* (18), 1900562.
17. Kellis, D. L.; Rehn, S. M., *et al.*, DNA-mediated excitonic upconversion FRET switching. *New Journal of Physics* **2015**, *17* (11), 115007.
18. Teitelboim, A.; Tian, B., *et al.*, Energy Transfer Networks within Upconverting Nanoparticles Are Complex Systems with Collective, Robust, and History-Dependent Dynamics. *The Journal of Physical Chemistry C* **2019**, *123* (4), 2678-2689.
19. LaBoda, C.; Duschl, H.; Dwyer, C. L., DNA-Enabled Integrated Molecular Systems for Computation and Sensing. *Accounts of Chemical Research* **2014**, *47* (6), 1816-1824.
20. Cannon, B. L.; Kellis, D. L., *et al.*, Excitonic AND logic gates on DNA brick nanobreadboards. *ACS photonics* **2015**, *2* (3), 398-404.
21. Graugnard, E.; Kellis, D. L., *et al.*, DNA-controlled excitonic switches. *Nano letters* **2012**, *12* (4), 2117-2122.
22. Buckhout-White, S.; Spillmann, C. M., *et al.*, Assembling programmable FRET-based photonic networks using designer DNA scaffolds. *Nature Communications* **2014**, *5*, 5615.
23. Yurke, B.; Turberfield, A. J., *et al.*, A DNA-fuelled molecular machine made of DNA. *Nature* **2000**, *406* (6796), 605.
24. Simmel, F. C.; Yurke, B.; Singh, H. R., Principles and Applications of Nucleic Acid Strand Displacement Reactions. *Chemical Reviews* **2019**, *119* (10), 6326-6369.
25. Limachia, M.; Thakker, R.; Kothari, N., A near-threshold 10T differential SRAM cell with high read and write margins for tri-gated FinFET technology. *Integration* **2018**, *61*, 125-137.
26. Parikh, P.; Senowitz, C., *et al.*, Three-dimensional nanoscale mapping of state-of-the-art field-effect transistors (FinFETs). *Microscopy and Microanalysis* **2017**, *23* (5), 916-925.

27. Fujii, R.; Nishimura, T.; Ogura, Y.; Tanida, J., Nanoscale energy-route selector consisting of multiple photo-switchable fluorescence-resonance-energy-transfer structures on DNA. *Optical Review* **2015**, 22 (2), 316-321.
28. Nishimura, T.; Ogura, Y.; Tanida, J., A nanoscale set–reset flip-flop in fluorescence resonance energy transfer-based circuits. *Applied Physics Express* **2012**, 6 (1), 015201.
29. Marras, S. A. E.; Kramer, F. R.; Tyagi, S., Efficiencies of fluorescence resonance energy transfer and contact- mediated quenching in oligonucleotide probes. *Nucleic acids research* **2002**, 30 (21), e122-e122.
30. LaBoda, C. D.; Lebeck, A. R.; Dwyer, C. L., An Optically Modulated Self-Assembled Resonance Energy Transfer Pass Gate. *Nano Letters* **2017**.
31. Bälter, M.; Hammarson, M., *et al.*, Reversible energy-transfer switching on a DNA scaffold. *Journal of the American Chemical Society* **2015**, 137 (7), 2444-2447.
32. Wu, Z.; Zhang, L., Photoregulation between small DNAs and reversible photochromic molecules. *Biomaterials Science* **2019**, 7 (12), 4944-4962.
33. Kellis, D. L.; Sarter, C., *et al.*, An All-Optical Excitonic Switch Operated in the Liquid and Solid Phases. *ACS Nano* **2019**, 13 (3), 2986-2994.

CHAPTER TWO: AN ALL-OPTICAL EXCITONIC SWITCH OPERATED IN THE  
LIQUID AND SOLID PHASES

This chapter is published by the American Chemical Society in ACS Nano and should be  
referenced appropriately.

Reference:

Kellis, D. L.; Sarter, C.; Cannon, B.L.; Davis, P. H.; Graugnard, E.; Lee, J.; Pensack, R.  
D.; Kolmar, T.; Jäschke, A.; Yurke, B.; Knowlton, W.B., An All-Optical Excitonic  
Switch Operated in the Liquid and Solid Phases, *ACS Nano* **2019**, 13 (3), 2986-2994.

Reproduction/modification by permission of the American Chemical Society.

\*This chapter includes modifications from the originally published version.



**AN ALL-OPTICAL EXCITONIC SWITCH OPERATED IN THE LIQUID  
AND SOLID PHASES**

Donald L. Kellis<sup>a</sup>

Christopher Sarter<sup>b</sup>

Brittany L. Cannon<sup>a</sup>

Paul H. Davis<sup>a</sup>

Elton Graugnard<sup>a</sup>

Jeunghoon Lee<sup>a,c</sup>

Ryan D. Pensack<sup>a</sup>

Theresa Kolmar<sup>b</sup>

Andres Jäschke<sup>b</sup>

Bernard Yurke<sup>a,d</sup>

William B. Knowlton<sup>a,d</sup>

<sup>a</sup>*Micron School of Materials Science & Engineering, Boise State University, Boise,  
Idaho, 83725, United States*

<sup>b</sup>*Institute of Pharmacy and Molecular Biotechnology, Heidelberg University, 69120,  
Heidelberg, Germany*

<sup>c</sup>*Department of Chemistry & Biochemistry, Boise State University, Boise, Idaho, 83725,  
United States*

<sup>d</sup>*Department of Electrical & Computer Engineering, Boise State University, Boise, Idaho,  
83725, United States*

## Abstract

The excitonic circuitry found in photosynthetic organisms suggests an alternative to electronic circuits, but the assembly of optically active molecules to fabricate even simple excitonic devices has been hampered by the limited availability of suitable molecular scale assembly technologies. Here we have designed and operated a hybrid all-optical excitonic switch comprised of donor/acceptor chromophores and photochromic nucleotide modulators assembled with nanometer scale precision using DNA nanotechnology. The all-optical excitonic switch was operated successfully in both liquid and solid phases, exhibiting high ON/OFF switching contrast with no apparent cyclic fatigue through nearly 200 cycles. These findings, combined with the switch's small footprint and volume, estimated low energy requirement, and potential ability to switch at speeds in the 10s of picoseconds, establish a prospective pathway forward for all-optical excitonic circuits.

## 2.1 Introduction

With the semiconductor industry rapidly approaching the end of Moore's law,<sup>1</sup> excitonics offers an attractive alternative to semiconductor electronics for information processing.<sup>2</sup> Excitonics exploits spatially proximate optically functional components<sup>3</sup> to capture and transport light energy below the diffraction limit of light. Natural light harvesting<sup>4, 5</sup> and photovoltaics,<sup>6</sup> as well as excitonic devices and logic gates<sup>7</sup> offer compelling examples of potential applications in excitonic circuit-based information processing. However, challenges to constructing technologically relevant excitonic circuits include identifying suitable: (i) substrates or scaffolds on which optically active components can be arranged into complex and scalable networks with nanometer scale

precision and control, and (ii) device architectures for gates that employ only excitons in their operation. While all-optical excitonic switches have been demonstrated using a photochromic moiety to modulate covalently attached donors in a process termed photochromic Förster resonance energy transfer (pcFRET),<sup>8, 9</sup> doing so on scaffolds in which optical components can be arranged in complex, well-defined, and scalable networks has yet to be achieved. Providing insight and inspiration to address these challenges are nature's photosynthetic organisms, which possess exquisite excitonic networks, such as light harvesting systems,<sup>4, 5</sup> that are >100 times smaller than the wavelength of visible light. Light harvesting systems employ proteins as a scaffold to self-assemble light active molecules, or chromophores, into excitonic networks that operate at room temperature in wet and noisy environments. The packing density of the chromophores is much higher than the component density of the most advanced electronic circuits, and exciton transport times rival electronic gate switching times.<sup>10</sup> However, self-assembly with proteins is very complicated owing to the over twenty amino acid protein building blocks and the difficulty of predicting *a priori* how peptide sequences will fold. In contrast, with only four nucleic acid building blocks and well-established design rules, DNA nanotechnology offers a more rational and feasible method of programmable self-assembly, with elegant control that yields exquisite one-, two-, and three-dimensional nanostructures.<sup>11, 12</sup>

Targeting the above-described challenges, various FRET-based excitonic devices have been developed, typically with donor/acceptor chromophore pairs self-assembled onto static or dynamic DNA scaffolds. These include switches,<sup>7, 13, 14</sup> logic gates,<sup>7, 15</sup> and energy ratchet switches.<sup>16</sup> However, the switching processes employed in these devices require aqueous solutions with chemical compositions that enable DNA duplex

dissociation *via* DNA strand invasion,<sup>17</sup> DNA-intercalation,<sup>18</sup> or chromophore modulation.<sup>19-24</sup> Furthermore, these switching processes have rate-limiting steps such as strand displacement, mass transport, and reducing agent diffusion which lead to challenges including cyclic fatigue and long cycle times (Supporting Information S1). Although excitonic switching performed in a liquid phase may be useful in super resolution imaging or medical diagnostics,<sup>25-27</sup> to create a viable excitonics technology, an all-optical switch operating in a solid phase is preferred.

A faster, more robust means of all-optical switching has become possible through recent developments for covalently integrating diarylethene photochromic units into DNA oligonucleotides.<sup>28-30</sup> The advantage of all-optical switching lays in the photophysics of ring opening and closing, that of photoisomerization, which is one of the fastest reactions studied to date.<sup>31</sup> Unique to this method is the integration of the nucleobase into the photochromic unit, enabling it to pair with complementary nucleotides (Supporting Information S2 and Scheme S1). Automated solid-phase phosphoramidite chemistry allows the synthesis of DNA oligonucleotides containing multiple photochromic units along the strand length on any desired nucleobase.

In this study, we used mono- and tri-diarylethene modified DNA oligonucleotides as optically reversible switching elements paired with donor/acceptor chromophores to create an all-optical excitonic switch. We exploited DNA self-assembly<sup>32, 33</sup> to fabricate an all-optical excitonic switch operable in both liquid and solid phase. Advancing functional molecular systems incorporated in DNA duplexes, the all-optical excitonic switch demonstrates exceptional switching contrast between the ON and OFF states with no evidence of cyclic fatigue. These findings, combined with the structural programmability

of DNA<sup>34, 35</sup> and the ability of photochromic nucleotides to switch at sub-nanosecond speeds<sup>36, 37</sup> (comparable to today's state-of-the-art transistors, signal a pathway for constructing all-optical excitonic circuits that are significantly smaller and faster than current electronic circuits.

## 2.2 Results and Discussion

### 2.2.1 Design

The optical switching elements of our device consist of a series of photochromic nucleotides assembled into the backbone of DNA oligonucleotides by chemical synthesis. Like natural nucleotides, these photochromic nucleotides comprise a deoxyribose sugar, a phosphate group, and a heterocyclic base capable of pairing with complementary nucleotides. However, the base is covalently modified to be part of a diarylethene photochromic unit.<sup>28-30</sup> Diarylethenes, originally developed for optical information storage purposes,<sup>38</sup> undergo a reversible photoinduced electro-cyclic ring closure reaction. Ultraviolet (UV) irradiation forms a colored closed-ring isomer, while irradiation at longer (visible) wavelengths leads to a colorless open-ring form, thereby rendering the nucleotide absorptive or transmissive to light of specific wavelengths, a property that is critical for our design. Depending on the chemical nature of the diarylethenes, switching can be fully reversible, and more than  $10^5$  cycles have been reported for some systems.<sup>39</sup> In the photochromic nucleotides used here, a uracil ring embedded in a DNA sequence is one of the aryl residues, attached *via* its 5-position to a cyclopentene-linked thiophene (Figure 2.3.1d and Supporting Information S2).<sup>29, 40</sup> The premise behind the design of our all-optical excitonic switch is that the photochromic nucleotide(s) will modulate (Supporting Information S1) the excitonic emission of both the donor and the acceptor when the donor,

photochromic nucleotide(s), and acceptor are all positioned within the Förster radius of each other. Based on the assumption that increasing the number of photochromic nucleotides present will increase the modulation of exciton flow and photon emission, the incorporation of both one and three photochromic nucleotides was examined (Figures 2.3.1a & 2.3.1b).

In the case of our all-optical excitonic switch, resonant energy transfer can occur either from donor to acceptor *or* from donor to photochromic nucleotide(s), which act as an alternate set of acceptor(s). FRET efficiency and excitonic transfer depend upon the properties of all chromophores involved in their respective transfer pathways. The properties that govern the relative FRET efficiency and excitonic transfer in the ON *vs.* OFF states are the inter-chromophore distances, spectral overlap of donor emission and acceptor absorption, and the relative orientations of the donor emission and acceptor absorption dipole moments.<sup>41</sup> The self-assembly of the all-optical excitonic switch device is illustrated in Figure 2.3.1c, wherein all positions (and hence inter-chromophore distances) are precisely controlled through sequence design (Supporting Information Table S1). The spectral overlap of both donor and acceptor along with donor and photochromic nucleotide are appropriately engineered in our design to achieve maximum modulation of both excitonic flow and photon emission (see Supporting Information S3 and Figure S1a). However, the chromophores used in this research have been attached to the ssDNA *via* single, flexible tethers; thus, achieving complete control over the relative dipole orientations of the optical switching elements is not possible.

For clarity in visualizing spectral overlap, normalized absorption (dashed curves) and emission (solid curves) spectra of the photochromic strand with three photochromic

units,<sup>29, 40</sup> ATTO 390 donor strand, and ALEXA 488<sup>42</sup> acceptor strand used in this study are shown in Figures 2.3.1d, 2.3.1e, and 2.3.1f, respectively. Unaltered absorbance spectra, also relevant to the absolute modulation efficiency, are provided in the Supporting Information (Figure S1b). The large absorbance below 300 nm is due solely to the DNA strands. The photochromic nucleotide can be cycled from the open non-visible light absorbing configuration (ON state - red dashed/dotted curve, Figure 2.3.1d) to the closed visible light absorbing configuration (OFF state - red dashed curve, Figure 2.1d) by exposure to 300 nm UV light, while cyclo-reversion is accomplished by exposing it to 455 nm visible (VIS) light. These wavelengths were chosen in order to: *i*) minimize damage to the DNA, which is known to occur with UV light of shorter wavelengths and *ii*) utilize wavelengths as close as possible to the absorption maxima of the photochromic nucleotide.

High-performance liquid chromatography (HPLC) was conducted in order to determine the maximal switching efficiency (*i.e.*, the photostationary state composition) of single photochromic nucleotide strands. Separation and identification of the two possible closed-ring isomers and one open-ring isomer in the HPLC data indicates a switching efficiency of  $50 \pm 2\%$  from the open to the closed form at the photostationary state and near unity conversion to the open form ( $<0.2\%$  closed form, below detectable limit) for closed to open switching (see Supporting Information S4, Figure S2, and Table S2). To minimize perturbation of the photochromic nucleotide during optical measurements, the donor was excited with 350 nm visible light (Figure 2.3.1e, donor absorption spectrum, blue dashed curve), resulting in donor emission (blue solid curve) with a maximum at 460 nm. The acceptor's absorption spectrum (Figure 2.3.1f, green dashed curve) overlaps the donor emission, resulting in FRET-based acceptor emission (green solid curve) at 520 nm.

Synthesis of a reversible photochromic moiety covalently bound to a nucleotide and incorporated into a single strand of DNA (ssDNA) (Figure 2.3.1d chemical structure insets) has been previously demonstrated,<sup>29</sup> however, integrating multiple diarylethene units into ssDNA, which is required to examine the selectivity of the all-optical excitonic switch, has remained elusive. The increased absorbance of one *versus* three photochromic nucleotides per strand is expected to produce a threefold increase in the donor/acceptor emission modulation (*i.e.*, selectivity, Supporting Information S5 and Figure S3). The relative absorbance of one *versus* three photochromic nucleotides (Figure 2.3.1g) indicates this assumption holds true, with the corresponding ON and OFF emission data shown in Figure 2.3.1h. Since inclusion of three photochromic nucleotides led to increased ON/OFF state contrast, all data presented here will be from the three photochromic nucleotide strand.



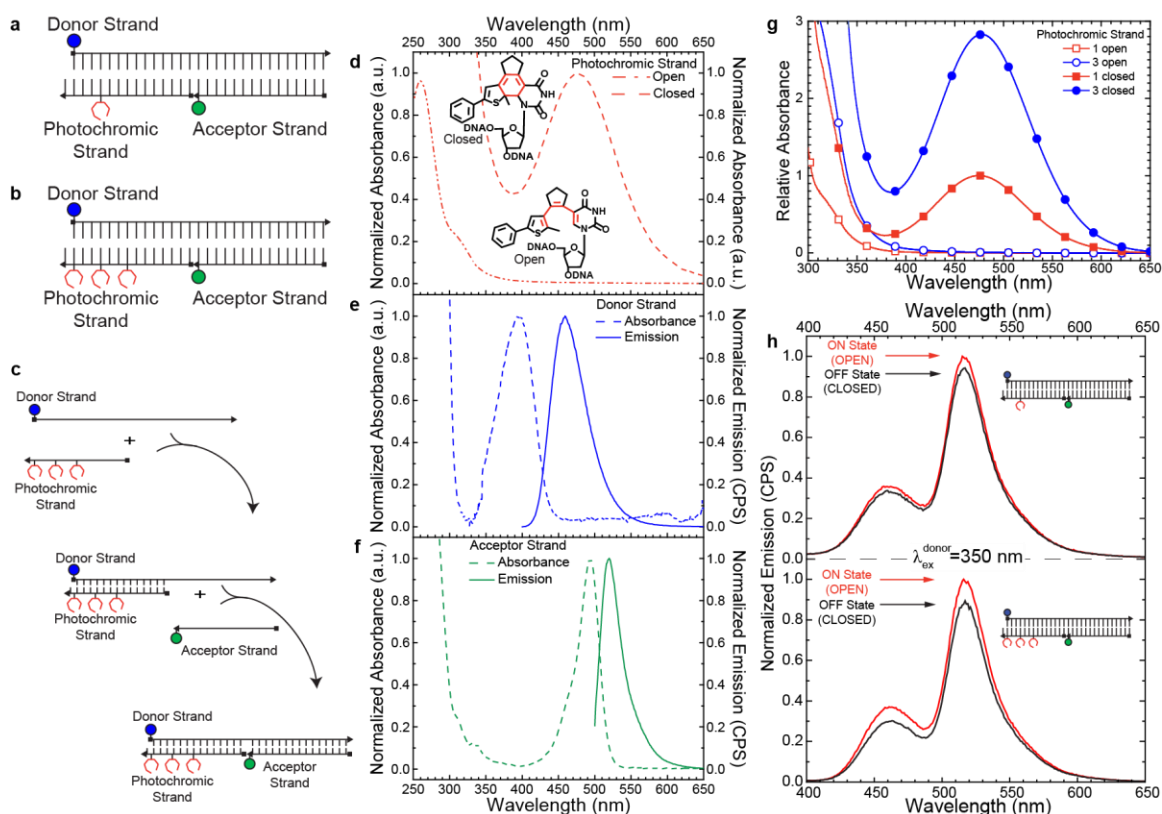


**Figure 2.1 All-optical excitonic switch design. (a, b) Schematic of the all-optical excitonic switch with one and three photochromic nucleotides, respectively. (c) Schematic of the self-assembly process allowing for precisely controlled placement of the optical components employed in the all-optical excitonic switch through binding domains. (d) Normalized absorption spectra of the photochromic strands in the CLOSED (absorbing) and OPEN (non-absorbing) configurations. Schematic insets illustrate molecular configuration changes occurring in the photochromic nucleotides with the ring system formed or opened highlighted in red. (e, f) Normalized absorption and emission spectra of the donor and acceptor strands, respectively, utilized in this study. (g) Relative absorbance spectra of photochromic strands containing a single photochromic nucleotide (design scheme 1a) versus three photochromic nucleotides (design scheme 1b), illustrating the three-fold increase in absorption (Supporting Information S5 and Figure S3). (h) Static emission plots of the all-optical excitonic switch in the ON and OFF state collected using the two design schemes (1a & 1b) from this study. Of note is the increased difference between the ON state and OFF state when the triple photochromic strand (lower plot) is employed, indicating improved excitonic modulation with design scheme 1b.**

### 2.3 Excitonic Modulation

Static and dynamic optical measurements were performed to assess FRET and excitonic emission modulation by monitoring changes in both the donor and acceptor emission with the photochromic nucleotides in either their open (ON) or closed (OFF) configuration (Supporting Information S6). For static measurements, the photochromic nucleotides were set to either an open or closed configuration. Conversely, dynamic measurements required the simultaneous light exposure of both the photochromic nucleotides (to initiate opening or closing) and excitation of the donor or acceptor while concurrently monitoring the donor or acceptor emission. Static emission spectra (Figures 2.4a & 2.4d) of the donor and acceptor strands were acquired by continuously exciting the donor strand. Figures 2.4a & 2.4d show an overall decrease in the static emission scans of the all-optical excitonic switch in the liquid and the solid phase, respectively, when the photochromic nucleotides are set to the OFF state, indicating they act to inhibit the donor and acceptor emission and abate the FRET process (Supporting Information S7 and Figure S5). Subtle variations in the emission intensities and slight absorbance shifts are noted (Figure 2.4d). Repeated cycling of the photochromic nucleotides between the open and closed configuration modulated the emission of both the donor and the acceptor (Figures 2.4a & 2.4d). Comparing the maximum donor and acceptor emission after each opening and closing event resulted in saw-tooth behavior (Figures 2.4b & 2.4e) with clear ON/OFF switching contrast indicative of modulation with minimal fluctuation. The static emission scans (Figures 2.4a & 2.4d) and saw-tooth behavior (Figures 2.4b & 2.4e) reinforce the hypothesis of modulation of FRET and excitonic emission as well as demonstrate

consistent resetting of the photochromic nucleotides between the open and closed configurations, validating successful all-optical excitonic switching.

The ability to observe real-time changes in the donor or acceptor emission while simultaneously changing/cycling the configuration (open or closed) of the photochromic nucleotides (*i.e.*, dynamic modulation emission scans) would provide insight into the dynamics of the all-optical excitonic switch (*i.e.*, dynamics of the ON and OFF states). Accordingly, dynamic modulation scans (Figures 2.4c & 2.4f) were performed by exposing the photochromic nucleotides while monitoring the donor or acceptor emission. Time dependent changes in the donor and the acceptor emission provide a convenient proxy to monitor the changes from ON to OFF or OFF to ON states (*e.g.*, fully *versus* partially ON or OFF) of the all-optical excitonic switch. From Figures 2.4c & 2.4f, time dependent exponential growth/decay of the donor and acceptor emission is observed as the photochromic nucleotides are excited over an exposure time of 30 seconds.

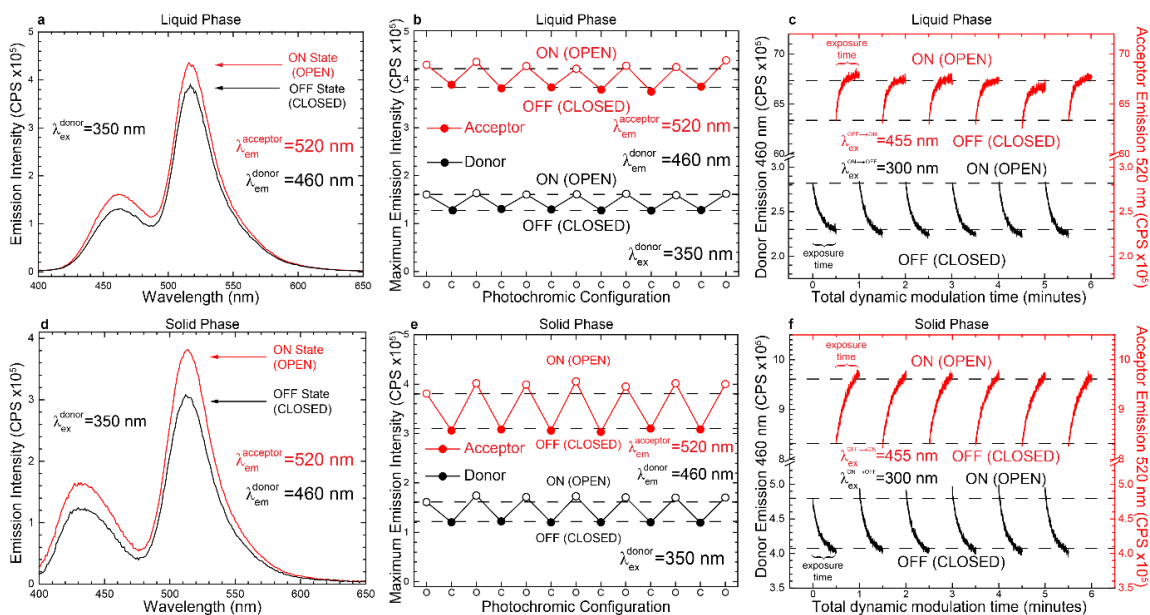


**Figure 2.2 All-optical excitonic switch emission. Emission modulation data for the all-optical excitonic switch with three photochromic nucleotides attached (as illustrated in Figure 1b) operated at concentrations of 20  $\mu\text{M}$  in the liquid (a-c) and 52 mM (calculated) in the solid (Supporting Information S8, Figure S6, and Table S3) (d-f) phases with an exposure time of 30 seconds. (a & d) Static emission plots of the all-optical excitonic switch in the ON and OFF states demonstrating modulation between the donor and the acceptor emission maxima. A blue shift in the solid phase donor emission is noted (Supporting Information S9). (b & e) Saw-tooth plots demonstrating the changes in the donor and acceptor emission as the photochromic nucleotides are cycled between the open (O) and closed (C) configuration (i.e. ON and OFF states) six times, with near complete resetting of the all-optical excitonic switch between each cycle (i.e., no evidence of cyclic fatigue). Dashed lines have been added to aid in visualizing an ON/OFF threshold between the open and closed configuration of the photochromic nucleotide for both the donor and acceptor emission. (c & f) Dynamic modulation emission plots of the donor and the acceptor strand as the photochromic nucleotides are cycled between the open and the closed configuration six times; exponential behavior indicates first-order reaction kinetics.**

## 2.4 Characteristic Switching Times

From the exponential behavior of the dynamic modulation scans (Figures 2.4c & 2.4f), rate constants can be extracted and used to predict the amplitude difference between the ON and OFF states of the saw-tooth plots (Figures 2.4b & 2.4e). The amplitude difference between the ON and OFF states also provides a means for obtaining a well-defined characteristic switching time ( $t_s$ ) based on knowledge of the incident light.

The exponential nature of the dynamic modulation behavior (Figures 2.4c & 2.4f) provides a method to determine the mean time for modulation ( $\tau_i$ ) occurring during the exposure time ( $t_e$ ) of the photochromic nucleotide and all-optical excitonic switch for two regimes: (i)  $\tau_i$  close ( $\tau_c$ ), the mean time to close the photochromic nucleotide when exposed at 300 nm, and (ii)  $\tau_i$  open ( $\tau_o$ ), the mean time to open the photochromic nucleotide when exposed at 455 nm. The sum of the two mean times for modulations,  $\tau_o$  and  $\tau_c$ , is defined as  $\tau_\Sigma$ , the time to complete one cycle from the ON state to the OFF state and back to the ON state.

As both the static and dynamic modulation emission scans exhibit modulation and the dynamic modulation emission data exhibit exponential behavior, we hypothesize that the changes in the maximum static emission intensities of the donor or acceptor (Figures 2.4b & 2.4e), termed the switching amplitude ( $\Delta_s$ ), is related to a well-defined characteristic switching time ( $t_s$ ) of the all-optical excitonic switch. Assuming a first order reaction rate, we derived the relationship between  $\Delta_s$  and  $t_e$  (Supporting Information S10 and S11) with only one modelling parameter and demonstrate the relationship holds over a range of  $t_e$ 's with the ability to extract  $t_s$ .

Plotting the switching amplitude ( $\Delta_s$ ) of the donor and acceptor emission collected from a series of time trial experiments (Figures 2.5a & 2.5d and Supporting Information S12 and Table S4) *versus* the photochromic nucleotide  $t_e$ 's (Figures 2.5c & 2.5f) enables modelling the time trial data using Equation 9 (Supporting Information S10). Because the dynamic modulation (Figures 2.5b & 2.5e) exhibits first order reaction kinetics behavior from which  $\tau_o$  and  $\tau_c$  can be extracted, the switching amplitude ( $\Delta_s$ ) may be assumed to become constant if  $t_e$  is sufficiently long; that is, if  $t_e$  is long enough, all (*i.e.*, a steady state

amount) of the photochromic nucleotides are cycled from one configuration to the other. Theoretically, the characteristic switching time ( $t_s$ ) is then equivalent to  $\tau_\Sigma$  (*i.e.*,  $\tau_o + \tau_e$ ) at the point when  $\Delta_s$  becomes constant (Supporting Information S11).

The data and the model (Figures 2.5c & 2.5f, Eq. 9 Supporting Information S10) show the predicted linear increase in  $\Delta_s$  in the range of ~ 1-10 seconds, transitioning to a constant  $\Delta_s$  between ~20-1000 seconds where the transition between linear and constant is defined as the “knee”. The intersection of tangent lines (not shown) of the linear and constant regions of  $\Delta_s$  gives  $t_s$  (dotted line Figures 2.5c & 2.5f), where  $t_s$  was found to be 17.0 and 23.3 seconds for the liquid and solid phases, respectively. The value of  $t_s$  *versus* the calculated (from Figures 2.5b & 2.5e) value of  $\tau_\Sigma$  (dashed line Figures 2.5c & 2.5f) results in a difference of approximately 17% for the liquid phase and 14% for the solid phase, which is in good agreement with our model (Eq. 9 Supporting Information S10). We note that for the solid phase model, the variation between the donor and the acceptor is much smaller than for the liquid phase model; this is attributed to the smaller difference between the dynamic modulation data as shown in Figure 2.5e.

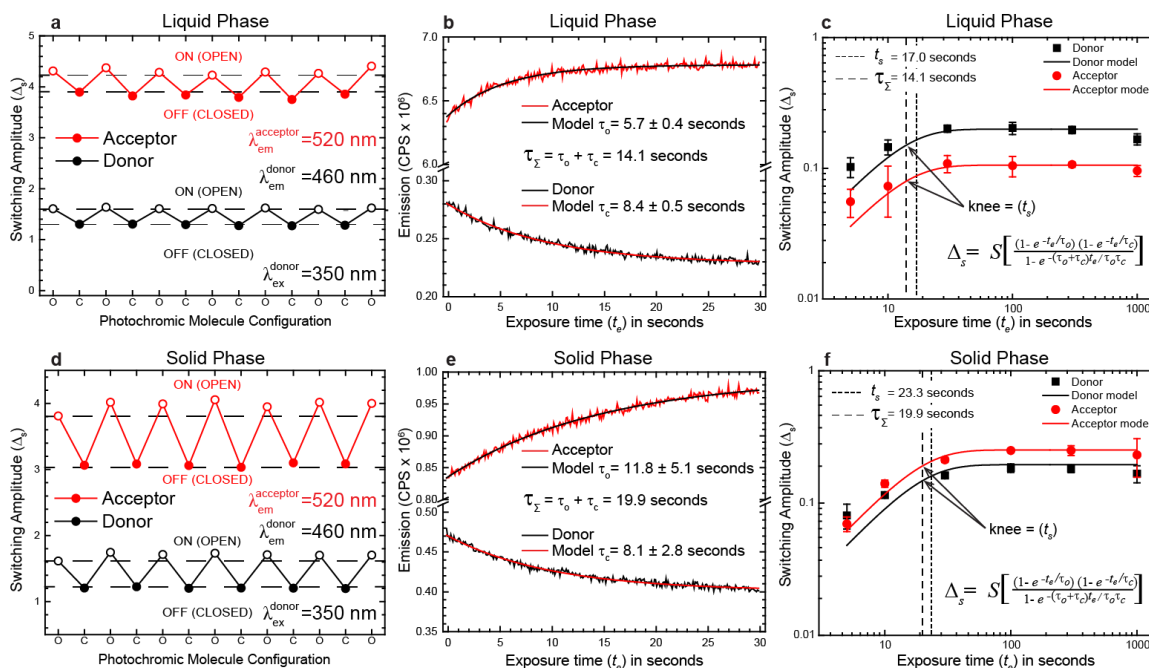


**Figure 2.3 Characteristic all-optical excitonic switch time. Characteristic switching time ( $t_s$ ) determination from the liquid and solid phase time trial experiments (a & d). Representative averaged saw-tooth plots extracted from 30 second exposure time liquid and solid phase time trial static emission scans (b & e). Representative dynamic modulation plots of the donor and acceptor emission by the photochromic nucleotides with exponential decay fits, extracted  $\tau_c$ ,  $\tau_o$ , &  $\tau_\Sigma$  times given (c & f). Switching amplitude ( $\Delta_s$ ) versus photochromic nucleotide exposure time ( $t_e$ ) of the photochromic nucleotides plotted with the first order reaction kinetics model (Eq. 9 Supporting Information S10). Error bars were generated from averaged standard deviations of each time trial  $\Delta_s$  series.**

To estimate how quickly the all-optical excitonic switch could in theory be cycled between the ON and OFF states, the absorbance cross section is required. The absorbance cross sections ( $\sigma$ ) of the all-optical excitonic switch were determined for the photochromic nucleotides in either the open or closed configuration using  $\tau_o$  and  $\tau_c$ , and were found to be  $7.7 \times 10^{-21}$  and  $1.4 \times 10^{-21}$  m<sup>2</sup>, (Eqs. 42 – 44 Supporting Information S13), respectively, which align closely to values reported for non-nucleosidic diarylethenes.<sup>43</sup> It should be noted that the values of  $\tau_o$ ,  $\tau_c$ ,  $\tau_\Sigma$ , and  $t_s$  determined from the time trial experiments are dependent upon the photon flux ( $2.3 \times 10^{19}$  m<sup>-2</sup>·s<sup>-1</sup> (CLOSE) and  $8.6 \times 10^{19}$  m<sup>-2</sup>·s<sup>-1</sup> (OPEN) of the incoherent Xenon light source used for this work, Supporting Information S14), and

ultimately limited by the detector integration time (0.1 seconds here). Given these dependencies and the extracted absorbance cross sections, our calculations (Supporting Information S15) show it should be possible to obtain a  $t_s$  in the picosecond range by using a high peak power ultrafast laser (*i.e.*, greater photon flux and shorter exposure time) with a photon flux of approximately  $10^{20}$  to  $10^{21}$   $\text{m}^{-2}$  per pulse. In fact, intrinsic cycle times on the order of picoseconds have been demonstrated for the opening and closing of non-nucleoside photochromic diarylethenes<sup>36, 37</sup>. As a frame of reference, this suggests the all optical switch has the potential to attain switching speeds similar to state-of-the-art transistors (Supporting Information S16, Table S5, and Table S6).

## 2.5 Cyclic Fatigue Assessment

To move toward technologically relevant all-optical excitonic switches, prolonged cycling with minimal cyclic fatigue (Supporting Information S1) is required.<sup>44</sup> To date, FRET-based optical switches and logic gates have shown, at most, twenty cycles,<sup>18, 45, 46</sup> after which cyclic fatigue ensues. Cycling of the all-optical excitonic switch between ON and OFF states while monitoring the acceptor emission in both the liquid and solid phase was performed nearly 200 times (Figure 2.6). The maximum random variation for either the ON or OFF states is |6%| or less, most likely due to thermal drift of the spectrometer. To minimize the effect of spectrometer drift, the insets in Figure 2.6 provide an alternate method to assess the variation in cycling by examining  $\Delta_s$  and the variation over five cycles in three separate time regions. In these three regions, the variation is very small ( $\leq 0.55\%$ ). Additionally, comparing  $\Delta_s$  and the variation within these three regions reveals values that are very similar, indicating no apparent evidence of cyclic fatigue. The absence of cyclic fatigue is most likely attributed to superior cyclic fatigue resistance of the diarylethene



photochromic nucleotide<sup>44, 47, 48</sup> as well as the photostability (Supporting Information S1) of the chromophore selection.<sup>49</sup> While future studies will be required to examine the overall reliability of our all-optical excitonic switch, the preliminary results for the all-optical excitonic switch demonstrate exceptional cyclic fatigue resistance in the liquid and solid phases, as well as over two orders of magnitude greater cycling when compared to other DNA scaffolded FRET-based excitonic switches.<sup>7, 13, 16, 18, 45, 46</sup>

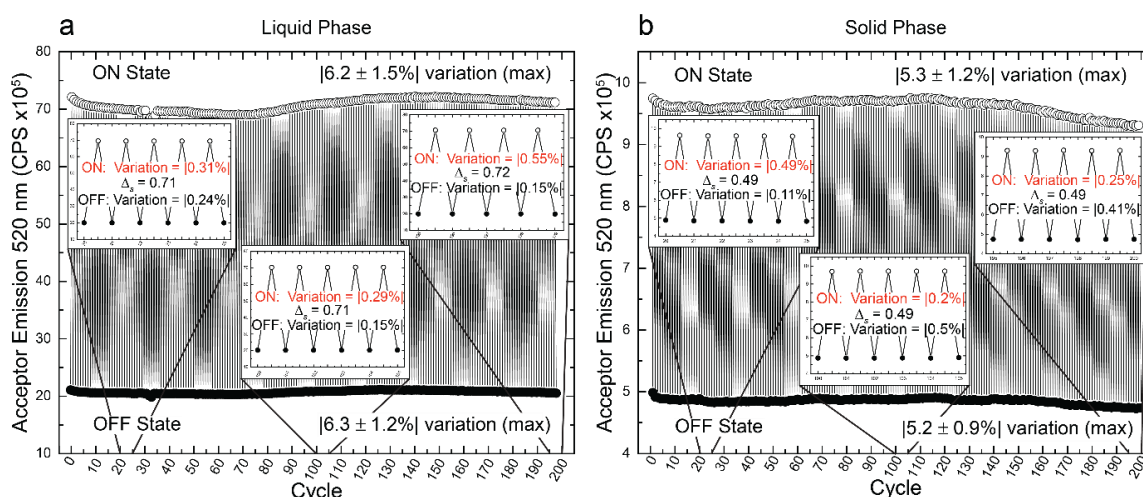


**Figure 2.4 Cyclic fatigue assessment.** Cycling of the all-optical excitonic switch operated at a concentration of 20  $\mu$ M in the liquid (a), and 52 mM in the solid (b) phases with an exposure time of 30 seconds performed nearly 200 times over the course of 100 minutes. Dynamic modulation scans were performed by exposing the photochromic nucleotides with ultraviolet (UV)  $\lambda_{ex}^{ON \rightarrow OFF}$  300nm or visible (VIS)  $\lambda_{ex}^{OFF \rightarrow ON}$  455nm light while monitoring the acceptor emission at 520 nm. Saw-tooth plots were created by averaging the final ten seconds of each cycling event to produce a single data point. About 6% or 5% random variation over the entire cycling range was determined for both the ON and OFF states in the liquid and the solid, respectively. Insets show that little cycle to cycle variation is observed, with values of both variation and  $\Delta_s$  exhibiting little change. No apparent cyclic fatigue is observed over the course of the trial within the resolution of the experiment.

## 2.6 Methods

### 2.6.1 Photochromic Nucleotide Synthesis

Commercially available reagents were purchased from Sigma Aldrich, Carbolution, and Carbosynth. These reagents and laboratory grade solvents were used without further

purification. Dry (moisture-free) solvents were purchased in sealed bottles packaged over molecular sieves. Solvents for oxygen-sensitive reactions were degassed prior to use by passing a continuous argon flow through the solvent for about 10 minutes. All reactions were monitored by thin layer chromatography (TLC) using silica plates coated with a fluorescent indicator and visualized with UV light (254 nm) or stained with a blue shift solution (ceric sulfate, molybdato-phosphoric acid, and sulfuric acid). Reactions under high pressure were conducted in microwave tubes sealed with a gas tight climber cap. Flash chromatography was performed with silica gel 60 (0.04-0.063 mm) using laboratory grade solvents. High-resolution mass spectra were recorded on a Bruker microTOF-Q II ESI (ESI). Nuclear magnetic resonance (NMR) spectra were recorded on Varian Systems 300 and 500 instruments with chemical shifts ( $\delta$ ) indicated in parts per million (ppm) downfield of tetramethylsilane (TMS) and referenced to the respective residual undeuterated solvent peak as follows:  $\text{CDCl}_3 = 7.26$  ppm,  $\text{MeOH-d}_4 = 3.31$  ppm for  $^1\text{H-NMR}$ ; and  $\text{CDCl}_3 = 77.0$  ppm,  $\text{MeOH-d}_4 = 49.00$  ppm for  $^{13}\text{C-NMR}$ . Apparent coupling constants ( $J_{\text{app}}$ ) are reported in Hz. (Supporting Information S17, Table S7, and Table S8).

### 2.6.2 Solid Phase Synthesis of Modified Oligonucleotides

The photochromic strands (PS1 and PS3) were synthesized by solid phase synthesis using phosphoramidite chemistry on an Expedite 8909 synthesizer. Reagents were purchased from Roth and Sigma Aldrich (Proligo) and used without further purification. A solid support 500 Å controlled pore glass (CPG) was used. The phosphoramidites of the four DNA-nucleosides (2'-deoxy-adenosine, -guanosine, -cytidine and -thymine) were dissolved in dry acetonitrile at a concentration of 0.075 M and molecular sieves (Roth, 4 Å, type 514) were added. The modified phosphoramidite (3) was dissolved in dry

acetonitrile at a concentration of 0.1 M. For the synthesis of the modified oligonucleotides, a standard 1  $\mu\text{mol}$ -protocol was used. After the synthesis, the oligonucleotide was deprotected and cleaved off the CPG using 25% ammonia (4 hrs, 40°C). The solid phase was washed with 25% ammonia (3 x 1 mL) and ultrapure water (3 x 1 mL) to remove the oligonucleotide completely from the solid support. The ammonia/water mixture was lyophilized, and the crude product was dissolved in water, filtered, and purified using preparative HPLC (PS1 with Method A and PS3 with Method B, (Supporting Table S9)). The product-containing fractions were lyophilized and their purity was analyzed by HPLC using Method C (Supporting Table S10).

### 2.6.3 HPLC Purification

HPLC purification and measurements were performed using an Agilent HP 1100 series machine equipped with a diode array detector (DAD) and processed using the ChemStation software. Purification was accomplished using a semi-preparative Luna 5u C18(2) 100A column (15 x 250 mm, Phenomenex) with a flowrate of 5 mL/min. As solvent, a mixture of Buffer A (0.1 M triethylammonium acetate in water, pH 7) and Buffer B (0.1 M triethylammonium acetate in 80% acetonitrile) was used (Supporting Information Table S9).

### 2.6.4 LC/MS Analysis

Liquid chromatography/mass spectrum (LC/MS) purification and measurements were carried out using an HP 1200 series HPLC from Agilent coupled to a microTOF-Q II ESI mass spectrometer (Bruker) and processed with the Hyphenation Star PP (Version 3.2.44.0) Software (Bruker Daltonics). A Kinetex 2.6  $\mu\text{m}$  C18 100 Å column (Phenomenex) was used. For the HPLC portion, Method C was employed, using a mixture of Buffer C

(100 mM hexafluoroisopropanol + 8.6 mM triethylamine, pH 8.3) and methanol (LC-MS grade, Sigma Aldrich). (Supporting Information Table S8, Table S10, and Figure S7)

#### 2.6.5 Single Stranded DNA (ssDNA) Sequence Design

The base sequences for the ATTO 390 donor and the ALEXA 488 acceptor ssDNA strands were designed using the web-based NUPACK (<http://nupack.org/>) program, which allowed for matching DNA bases to the custom photochromic nucleotide strand (Supporting Information Table S1). Furthermore, NUPACK provided thermodynamic analysis to determine the lowest free energy of the fully hybridized double stranded DNA structure. The sequences for the chromophore labeled (i.e., donor and acceptor), photochromic strands (photochromic nucleotide dUPS given in red), and control (i.e., bare) oligomers are given in Supporting Information Table S1. Donor and acceptor chromophore strands were purchased as lyophilized powders from BioSynthesis (Lewisville, TX, USA) with an initial synthesis scale at 1.0 optical density (OD) purified using dual high performance liquid chromatography (HPLC). Control strands were purchased lyophilized from Integrated DNA Technologies (Coralville, IA, USA) with an initial synthesis scale at 250 nmole purified with a standard desalting process. All strands were re-hydrated using ultrapure water (Barnstead Nanopure, Thermo Scientific) to a nominal 100  $\mu$ M stock concentration and used without further purification.

#### 2.6.6 Spectral Overlap Design

Spectral overlap is required between all optical molecules involved in the FRET and excitonic transfer processes. Sufficient overlap between the emission spectrum of the donor and the absorption spectrum of the acceptor must be present. Furthermore, the absorption spectrum of the photochromic nucleotide must coincide with both the emission

of the donor and the absorption of the acceptor. (Supporting Information S3 and Figure S1).

#### 2.6.7 All-optical Switch Hybridization.

Hybridization was performed with all ssDNA in 1x TAE buffer (40 mM tris(hydroxymethyl)aminomethane, 20 mM acetic acid, 2 mM ethylenediaminetetraacetic acid (EDTA); pH 8.0) with 15 mM magnesium acetate tetrahydrate ( $Mg^{2+}$ ) added at working DNA concentrations of 5  $\mu$ M or 20  $\mu$ M. The all-optical excitonic switch devices were constructed *via* self-assembly by combining all strands at equimolar concentration in a microcentrifuge tube and allowing ~15 minutes of hybridization time at room temperature, then testing without further modification or purification. When the three strands hybridize, a linear excitonic transmission line approximately 4.76 nm in length is formed, placing all of the optical active components within their Förster distances.

#### 2.6.8 Fluorescence Measurements.

Optical characterization involving acquisition of both the absorbance and fluorescence spectra of the all-optical excitonic switch was performed. UV-Vis absorbance spectra were collected for each individual strand using a dual-beam Cary 5000 UV-Vis-NIR spectrophotometer (Agilent Technologies) by pipetting 50  $\mu$ L of sample into a black-mask, 1 cm path length, low head space, sub-micro quartz cuvette (Cat. # 26.LHS-Q-10/Z20, Starna Cells). Static and dynamic emission spectra were collected using a Fluorolog-3 spectrofluorometer (HORIBA Scientific). Liquid phase data were obtained by pipetting 50  $\mu$ L of the all-optical excitonic switch solution into a black-mask, 1 cm path length, sub-micro fluorometer quartz cuvette (Cat. # 16.40F-Q-10/Z15, Starna Cells). Solid phase data were obtained by pipetting 5  $\mu$ L of the all-optical excitonic switch solution onto

a fused quartz microscope slide (Chemglass Life Sciences, USA) and placing it in a custom built vacuum chamber at 0.24 Torr for twelve hours. Quartz slides were cleaned prior to sample deposition by sonication in 2% Hellmanex (Hellma Analytics) solution for 5 minutes, followed by sonication in ultrapure water for 5 minutes and drying with ultra-high purity nitrogen (UHP, 99.999%). Fluorescence emission detector geometries are illustrated in Supporting Information Figure S4.

#### 2.6.9 Dynamic Modulation Measurements.

Dynamic measurements require the simultaneous light exposure of both the photochromic nucleotides (to initiate opening or closing) and excitation of the donor or acceptor while concurrently monitoring the donor or acceptor emission. Dynamic modulation scans (Manuscript Figures 2.2c & 2.2f) were performed by exposing the photochromic nucleotides with ultraviolet (UV)  $\lambda_{ex}^{ON \rightarrow OFF}$  300nm or visible (VIS)  $\lambda_{ex}^{OFF \rightarrow ON}$  455nm light while monitoring the donor or acceptor emission at 460 nm or 520 nm, respectively. Either the donor or the acceptor emission can be examined real-time while simultaneously opening or closing the photochromic nucleotides.

### **2.7 Conclusion**

While other scalable all-optical excitonic switches require specific aqueous solutions to operate and show cyclic fatigue after limited cycling, this work demonstrates a scalable all-optical excitonic switch that: (i) operates in both the liquid and solid phase, (ii) exhibits at least two orders of magnitude greater cycling, and (iii) yields high ON/OFF switching contrast with no evidence of cyclic fatigue. Simple approximations (Supporting Information S16, Tables S5, and Table S6) show that the all-optical excitonic switch has a 37x smaller footprint, over 3 orders of magnitude smaller volume, and requires over an

order of magnitude less cycling energy than a low power 14 nm FinFET, a current state-of-the-art MOSFET. Furthermore, estimated picosecond cycle times of the all-optical excitonic switch based on the underlying photophysics of diarylethenes strongly suggest that the all-optical excitonic switch could operate at speeds similar to current transistor technology. Based on our results and these calculations, the switch described here may be a powerful component of future molecular excitonic integrated circuits.

### **2.8 Author Justifications**

The experimental work presented in this publication was a collaborative effort by Donald L. Kellis and Christopher Sarter.

Donald L. Kellis contributed as the lead author of the manuscript. Donald performed the fabrication as well as the static and dynamic data collection of the all-optical excitonic switch. Donald L. Kellis's research contribution was a partial fulfillment of the requirements for a Master of Science degree in Materials Science and Engineering at Boise State under the advisement of Professor William B. Knowlton and Dr. Bernard Yurke.

Christopher Sarter (Graduate Student, Heidelberg University) contributed significantly through his synthesis, attachment, and purification of all diarylethene modified DNA oligonucleotides. Christopher Sarter's research contribution was a partial fulfillment of the requirements of the Doctor of Philosophy from Heidelberg University under the advisement of Dr. Andres Jäschke.

Theresa Kolmer (Graduate Student, Heidelberg University) contributed through her work in determination of the switching efficiency of the diarylethene modified DNA oligonucleotides.

Dr. Bernard Yurke (Distinguished Research Fellow, Boise State University) contributed significantly through his development of the switching time derivation, characteristic switching time derivation, and the time trial model. He also co-conceived the project and co-supervised the research being performed by Donald L. Kellis.

Dr. William B. Knowlton (Professor, Boise State University) contributed significantly through his development of the all-optical excitonic switch comparison to current state-of-the-art FinFET technologies. He also co-conceived the project and co-supervised the research being performed by Donald L. Kellis.

Drs. Paul H. Davis (Senior Research Scholar, Boise State University) and Ryan Pensack (Senior Research Scholar, Boise State University) contributed significantly to this work through their determination of ultrafast switching of the all-optical excitonic switch.

Dr. Andres Jäschke (Professor, Heidelberg University) contributed significantly to this work through his development of diarylethene modified DNA oligonucleotides. He also co-conceived the project and co-supervised the research being performed by Christopher Sarter.

All authors contributed to the design of experiments, data analysis, discussion, and manuscript editing.



## 2.9 Acknowledgements

This work was supported in part by the Boise State University Division of Research and Economic Development. The authors thank the students, staff, and faculty within the Nanoscale Materials & Device group for valuable assistance with this work as well as Jonathan Huff, and Christopher Green for thoughtful discussions. DLK acknowledges Dr. Amy Moll (Boise State University) for her support. We would like to thank Dr. Richard G. Southwick III for his help with and fruitful discussions concerning the FinFET calculations.

## References

1. Waldrop, M. M., More Than Moore. *Nature* **2016**, *530*, 144-148.
2. Szaciłowski, K., Digital Information Processing in Molecular Systems. *Chem. Rev.* **2008**, *108* (9), 3481-3548.
3. Boulais, É.; Sawaya, N. P. D.; Veneziano, R.; Andreoni, A.; Banal, J. L.; Kondo, T.; Mandal, S.; Lin, S.; Schlau-Cohen, G. S.; Woodbury, N. W., Programmed Coherent Coupling in a Synthetic DNA-Based Excitonic Circuit. *Nat. Mater.* **2018**, *17*, 159.
4. Green, B.; Parson, W. W., *Light-Harvesting Antennas in Photosynthesis*. Springer: New York, 2003; Vol. 13., pp 2-28.
5. Blankenship, R. E., *Molecular Mechanisms of Photosynthesis*. Wiley & Sons: Hoboken, 2014; pp 59-87.
6. Hedley, G. J.; Ruseckas, A.; Samuel, I. D. W., Light Harvesting for Organic Photovoltaics. *Chem. Rev.* **2017**, *117*, 796-837.
7. Cannon, B. L.; Kellis, D. L.; Davis, P. H.; Lee, J.; Kuang, W.; Hughes, W. L.; Graugnard, E.; Yurke, B.; Knowlton, W. B., Excitonic and Logic Gates on DNA Brick Nanobreadboards. *ACS Photonics* **2015**, *2*, 398-404.
8. Giordano, L.; Jovin, T. M.; Irie, M.; Jares-Erijman, E. A., Diheteroarylethenes as Thermally Stable Photoswitchable Acceptors in Photochromic Fluorescence Resonance Energy Transfer (PcFRET). *J. Am. Chem. Soc.* **2002**, *124*, 7481-7489.

9. Song, L.; Jares-Erijman, E. A.; Jovin, T. M., A Photochromic Acceptor as a Reversible Light-Driven Switch in Fluorescence Resonance Energy Transfer (FRET). *J. Photochem. Photobiol., A* **2002**, *150*, 177-185.
10. Scholes, G. D.; Fleming, G. R.; Olaya-Castro, A.; Van Grondelle, R., Lessons from Nature About Solar Light Harvesting. *Nat. Chem.* **2011**, *3*, 763.
11. Ke, Y.; Ong, L. L.; Shih, W. M.; Yin, P., Three-Dimensional Structures Self-Assembled from DNA Bricks. *Science* **2012**, *338*, 1177-1183.
12. Ong, L. L.; Hanikel, N.; Yaghi, O. K.; Grun, C.; Strauss, M. T.; Bron, P.; Lai-Kee-Him, J.; Schueder, F.; Wang, B.; Wang, P.; Kishi, J. Y.; Myhrvold, C.; Zhu, A.; Jungmann, R.; Bellot, G.; Ke, Y.; Yin, P., Programmable Self-Assembly of Three-Dimensional Nanostructures from 10,000 Unique Components. *Nature* **2017**, *552*, 72-73.
13. Graugnard, E.; Kellis, D. L.; Bui, H.; Barnes, S.; Kuang, W.; Lee, J.; Hughes, W. L.; Knowlton, W. B.; Yurke, B., DNA-Controlled Excitonic Switches. *Nano Lett.* **2012**, *12*, 2117-2122.
14. Buckhout-White, S.; Spillmann, C. M.; Algar, W. R.; Khachatryan, A.; Melinger, J. S.; Goldman, E. R.; Ancona, M. G.; Medintz, I. L., Assembling Programmable FRET-Based Photonic Networks Using Designer DNA Scaffolds. *Nat. Commun.* **2014**, *5*, 5615.
15. Nishimura, T.; Fujii, R.; Ogura, Y.; Tanida, J., Optically Controllable Molecular Logic Circuits. *Appl. Phys. Lett.* **2015**, *107*, 013701.
16. Kellis, D. L.; Rehn, S. M.; Cannon, B. L.; Davis, P. H.; Graugnard, E.; Lee, J.; Yurke, B.; Knowlton, W. B., DNA-Mediated Excitonic Upconversion FRET Switching. *New J. Phys.* **2015**, *17*, 115007.
17. Yurke, B.; Turberfield, A. J.; Mills Jr, A. P.; Simmel, F. C.; Neumann, J. L., A DNA-Fuelled Molecular Machine Made of DNA. *Nature* **2000**, *406*, 605.
18. Bälter, M.; Hammarson, M.; Remón, P.; Li, S.; Gale, N.; Brown, T.; Andréasson, J., Reversible Energy-Transfer Switching on a DNA Scaffold. *J. Am. Chem. Soc.* **2015**, *137*, 2444-2447.
19. Rust, M. J.; Bates, M.; Zhuang, X., Sub-Diffraction-Limit Imaging by Stochastic Optical Reconstruction Microscopy (STORM). *Nat. Methods* **2006**, *3*, 793.

20. Bates, M.; Huang, B.; Dempsey, G. T.; Zhuang, X., Multicolor Super-Resolution Imaging with Photo-Switchable Fluorescent Probes. *Science* **2007**, *317*, 1749-1753.
21. Dempsey, G. T.; Bates, M.; Kowtoniuk, W. E.; Liu, D. R.; Tsien, R. Y.; Zhuang, X., Photoswitching Mechanism of Cyanine Dyes. *J. Am. Chem. Soc.* **2009**, *13*, 18192-18193.
22. Dempsey, G. T.; Vaughan, J. C.; Chen, K. H.; Bates, M.; Zhuang, X., Evaluation of Fluorophores for Optimal Performance in Localization-Based Super-Resolution Imaging. *Nat. Methods* **2011**, *8*, 1027.
23. Fujii, R.; Nishimura, T.; Ogura, Y.; Tanida, J., Nanoscale Energy-Route Selector Consisting of Multiple Photo-Switchable Fluorescence-Resonance-Energy-Transfer Structures on DNA. *Opt. Rev.* **2015**, *22*, 316-321.
24. LaBoda, C. D.; Lebeck, A. R.; Dwyer, C. L., An Optically Modulated Self-Assembled Resonance Energy Transfer Pass Gate. *Nano Lett.* **2017**, *22*, 3775-3781.
25. Yuan, L.; Lin, W.; Chen, B.; Xie, Y., Development of FRET-Based Ratiometric Fluorescent Cu<sup>2+</sup> Chemodosimeters and the Applications for Living Cell Imaging. *Org. Lett.* **2011**, *14*, 432-435.
26. Wang, H.; Li, Y.; Xu, S.; Li, Y.; Zhou, C.; Fei, X.; Sun, L.; Zhang, C.; Li, Y.; Yang, Q., Rhodamine-Based Highly Sensitive Colorimetric Off-on Fluorescent Chemosensor for Hg<sup>2+</sup> in Aqueous Solution and for Live Cell Imaging. *Org. Biomol. Chem.* **2011**, *9*, 2850-2855.
27. Wu, W.-L.; Wang, Z.-Y.; Dai, X.; Miao, J.-Y.; Zhao, B.-X., An Effective Colorimetric and Ratiometric Fluorescent Probe Based FRET with a Large Stokes Shift for Bisulfite. *Sci. Rep.* **2016**, *6*, 25315.
28. Singer, M.; Jäschke, A., Reversibly Photoswitchable Nucleosides: Synthesis and Photochromic Properties of Diarylethene-Functionalized 7-Deazaadenosine Derivatives. *J. Am. Chem. Soc.* **2010**, *132*, 8372-8377.
29. Cahová, H.; Jäschke, A., Nucleoside-Based Diarylethene Photoswitches and Their Facile Incorporation into Photoswitchable DNA. *Angew. Chem., Int. Ed.* **2013**, *52*, 3186-3190.

30. Sarter, C.; Heimes, M.; Jäschke, A., The Role of Alkyl Substituents in Deazaadenine-Based Diarylethene Photoswitches. *Beilstein J. Org. Chem.* **2016**, *12*, 1103.
31. Schoenlein, R. W.; Peteanu, L. A.; Mathies, R. A.; Shank, C. V., The First Step in Vision: Femtosecond Isomerization of Rhodopsin. *Science* **1991**, *254*, 412-415.
32. Pilo-Pais, M.; Acuna, G. P.; Tinnefeld, P.; Liedl, T., Sculpting Light by Arranging Optical Components with DNA Nanostructures. *MRS Bull.* **2017**, *42*, 936-942.
33. Castro, C. E.; Dietz, H.; Högberg, B., DNA Origami Devices for Molecular-Scale Precision Measurements. *MRS Bull.* **2017**, *42*, 925-929.
34. Gopinath, A.; Miyazono, E.; Faraon, A.; Rothmund, P. W. K., Engineering and Mapping Nanocavity Emission Via Precision Placement of DNA Origami. *Nature* **2016**, *535*, 401.
35. Simmel, F. C.; Schulman, R., Self-Organizing Materials Built with DNA. *MRS Bull.* **2017**, *42*, 913-919.
36. Miyasaka, H.; Araki, S.; Tabata, A.; Nobuto, T.; Malaga, N.; Irie, M., Picosecond Laser Photolysis Studies on Photochromic Reactions of 1, 2-Bis (2, 4, 5-Trimethyl-3-Thienyl) Maleic Anhydride in Solutions. *Chem. Phys. Lett.* **1994**, *230*, 249-254.
37. Miyasaka, H.; Nobuto, T.; Itaya, A.; Tamai, N.; Irie, M., Picosecond Laser Photolysis Studies on a Photochromic Dithienylethene in Solution and in Crystalline Phases. *Chem. Phys. Lett.* **1997**, *269*, 281-285.
38. Irie, M., Diarylethenes for Memories and Switches. *Chem. Rev.* **2000**, *100*, 1685-1716.
39. Irie, M., Photochromism of Diarylethene Single Molecules and Single Crystals. *Photochem. Photobiol. Sci.* **2010**, *9*, 1535-1542.
40. Buckup, T.; Sarter, C.; Volpp, H.-R.; Jäschke, A.; Motzkus, M., Ultrafast Time-Resolved Spectroscopy of Diarylethene-Based Photoswitchable Deoxyuridine Nucleosides. *J. Phys. Chem. Lett.* **2015**, *6*, 4717-4721.
41. Scholes, G. D., Long-Range Resonance Energy Transfer in Molecular Systems. *Annu. Rev. Phys. Chem.* **2003**, *54*, 57-87.
42. Sabnis, R. W., *Handbook of Fluorescent Dyes and Probes*. Wiley & Sons: Hoboken, 2015; pp 20-22.

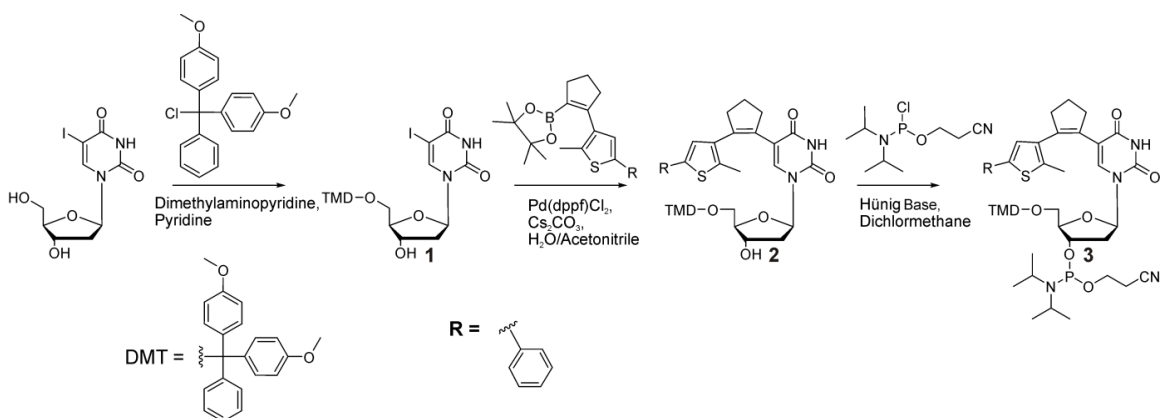
43. Pärs, M.; Hofmann, C. C.; Willinger, K.; Bauer, P.; Thelakkat, M.; Köhler, J., An Organic Optical Transistor Operated under Ambient Conditions. *Angew. Chem.* **2011**, *123*, 11607-11610.
44. Herder, M.; Schmidt, B. M.; Grubert, L.; Pätzelt, M.; Schwarz, J.; Hecht, S., Improving the Fatigue Resistance of Diarylethene Switches. *J. Am. Chem. Soc.* **2015**, *137*, 2738-2747.
45. Nishimura, T.; Ogura, Y.; Tanida, J., Fluorescence Resonance Energy Transfer-Based Molecular Logic Circuit Using a DNA Scaffold. *Appl. Phys. Lett.* **2012**, *101*, 233703.
46. Dryza, V.; Smith, T. A.; Bieske, E. J., Blue to near-Ir Energy Transfer Cascade within a Dye-Doped Polymer Matrix, Mediated by a Photochromic Molecular Switch. *Phys. Chem. Chem. Phys.* **2016**, *18*, 5095-5098.
47. Lucotti, A.; Bertarelli, C.; Zerbi, G., Optical Fatigue in a Solid State Diarylethene Polymer. *Chem. Phys. Lett.* **2004**, *392*, 549-554.
48. Hanazawa, M.; Sumiya, R.; Horikawa, Y.; Irie, M., Thermally Irreversible Photochromic Systems. Reversible Photocyclization of 1, 2-Bis (2-Methylbenzo [B] Thiophen-3-Yl) Perfluorocycloalkene Derivatives. *J. Chem. Soc., Chem. Commun.* **1992**, 206-207.
49. Spence, M. T. Z.; Johnson, I. D., *The Molecular Probes Handbook: A Guide to Fluorescent Probes and Labeling Technologies*. Life Technologies Corporation: Carlsbad, 2010; p 35.

### 3.0 Supporting Information

#### 3.1 Switching contrast, cyclic fatigue, cycle time, modulation, and photostability

We define the following terms for the discussion of the all-optical excitonic switch. ON/OFF switching contrast denotes the difference between the ON state static emission and the OFF state static emission of either the donor or the acceptor. Cyclic fatigue indicates any undesirable changes in the donor or the acceptor emission as a result of repeated ON/OFF cycling. Cycle time describes the time of exposure to a given wavelength of light (*i.e.*, 300 nm or 455 nm) used to cycle the all-optical excitonic switch between the closed or open configurations, respectively. Modulation refers to a statistically significant variation in donor or acceptor emission between the ON and OFF states. Photostability refers to the limited irreversible degradation of chromophores.

#### 3.2 Synthesis of the phosphoramidite for solid phase synthesis



**Scheme 3.1** Reaction pathway to synthesize the photoswitchable phosphoramidite building block (3) needed for solid phase synthesis.

**Table 3.1** Single strand DNA sequences

Strand Name	Sequence (5' to 3')	Length (nt)	Purification
Photochromic Strand (1) – PS1	GGCTAGCTACdU <sup>PS</sup> ACGA	15	HPLC*
Photochromic Strand (3) – PS3	GGCTAGCdU <sup>PS</sup> ACdU <sup>PS</sup> ACdU <sup>PS</sup> A	15	HPLC*
Donor Strand	/A390/AGTAGTAGCTAGCCGCACGCACCGGCTCG	29	Dual HPLC*
Acceptor Strand	CGAGCCGGTGCGTGC/A488/	15	Dual HPLC*
Photochromic (control)	GGCTAGCTACTACTA	15	Standard Desalting**
Donor (control)	AGTAGTAGCTAGCCGCACGCACCGGCTCG	29	Standard Desalting**
Acceptor (control)	CGAGCCGGTGCGTGC	15	Standard Desalting**

\*High-Performance Liquid Chromatography

\*\*Desalting to remove short products and small organic contaminants. Does not include polyacrylamide gel electrophoresis (PAGE) purification.

The common name and structure of the chromophores used in this study are:

ATTO 390: (2,5-dioxopyrrolidin-1-yl) 4-(4,6,8,8-tetramethyl-2-oxo-6,7-dihydroprano[3,2-g]quinolin-9-yl)butanoate.

ALEXA 488: Xanthylium, 3,6-diamino-9-[2-carboxy-4(*or* 5)-[(2,5-dioxo-1-pyrrolidinyl)oxy]carbonyl]phenyl]-4,5-disulfo-, inner salt, lithium salt (1:2) (39).

### 3.3 Normalized and unaltered spectral overlap data and chromophore selection

As indicated by the corresponding arrows in Figure 3.1a, which presents normalized absorption and emission spectra of all chromophores present in the all-optical excitonic switch, the chromophores were selected such that facile excitonic transfer occurs between the ATTO 390 donor emission ( $\lambda_{\text{max}} = 460$  nm, solid blue curve) and Alexa 488 acceptor absorption ( $\lambda_{\text{max}} = 495$  nm, dashed green curve). Additionally, the donor emission and the acceptor absorption fall well within the broad absorption band of the photochromic nucleotide when it is in the closed (“OFF” state) configuration (Fig. 3.1a, red dashed curve, 388 – 550 nm). For additional clarity in understanding the relative absorbance of the acceptor and photochromic nucleotide moieties, which affects the overall switching efficiency (*i.e.*, FRET modulation) of the all-optical excitonic switch, Figure 3.1b presents the unaltered (*i.e.*, non-normalized) absorption spectra of the Alexa 488 acceptor strand as well as the three photochromic nucleotide switch in its open and closed configurations, with the peak emission wavelength of the ATTO 390 donor indicated. Note that the absorbance of the photochromic nucleotides is ~6x less than that of the acceptor at the donor’s emission maximum, which leads to incomplete FRET quenching in the all-optical excitonic switch’s OFF state (*i.e.*, partial modulation of the fluorescence emission).



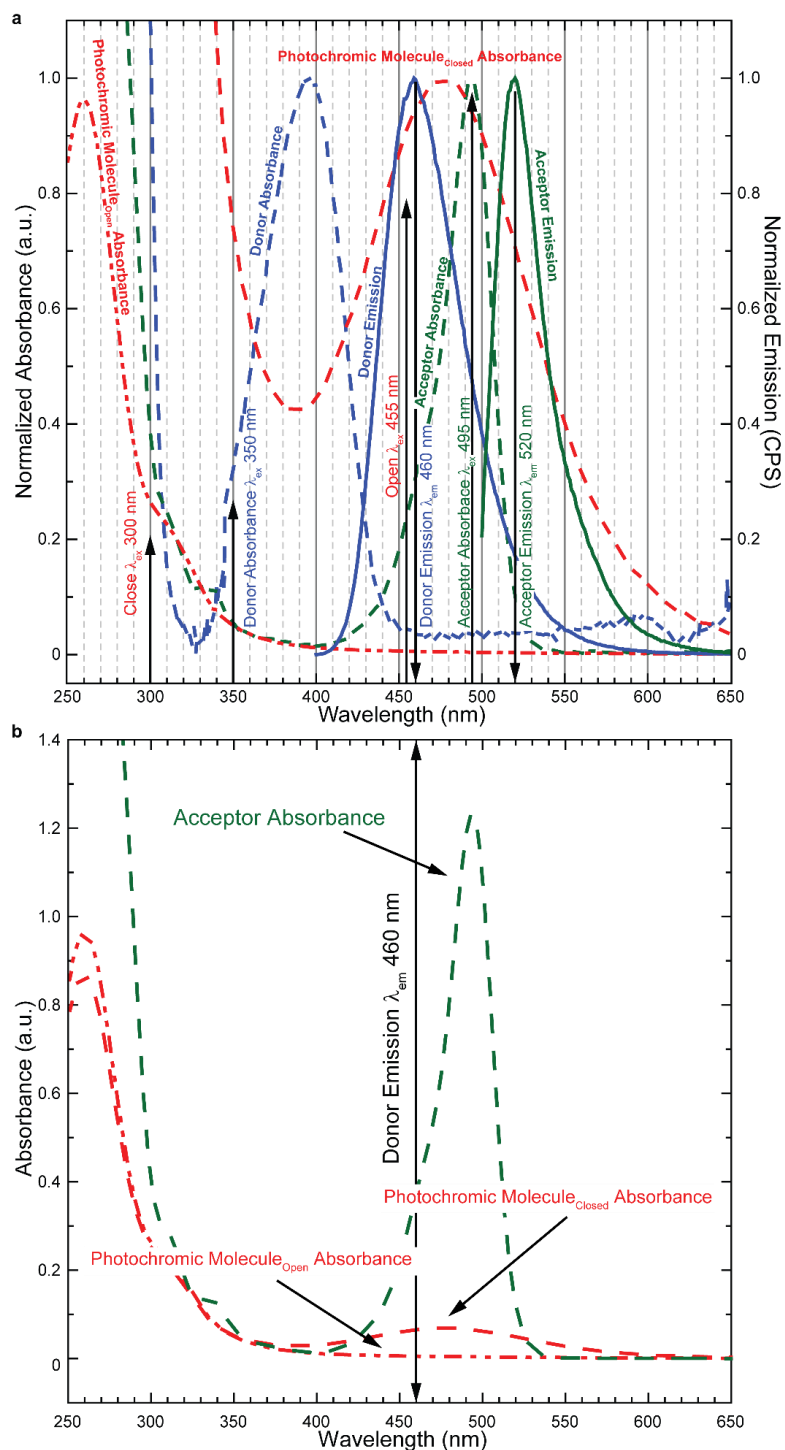


**Figure 3.1** Spectral overlap of the optical components comprising the all-optical excitonic switch. (a) Shown are the normalized absorption and emission spectra of the donor strand (blue dashed and solid curves, respectively), normalized absorption spectra of the photochromic nucleotides in both the open (non-absorbing, red dashed/dotted curve) and closed (absorbing, red dashed curve) configurations, and normalized absorption and emission spectra of the acceptor strand (green dashed and solid curves, respectively). Optical molecules were selected

such that overlap occurred among the donor emission, photochromic nucleotide closed configuration absorption, and acceptor absorption in order to modulate both the excitonic transfer and FRET processes. Exposure wavelengths were chosen such that minimal perturbation to the configuration of the photochromic nucleotides would occur during data collection. Up arrows indicate the wavelengths used to expose the optical molecule and the down arrow indicates the wavelength used to collect spectral data. The spectra have been normalized in order to easily visualize the spectral overlap in the 350-550 nm region. (b) The actual unaltered absorbance of the acceptor as well as the three photochromic nucleotides in their open and closed states. A comparison of the spectra highlights that the absorbance of the three photochromic nucleotides at the donor emission maximum ( $\lambda_{\text{max}} = 460 \text{ nm}$ ) is approximately 6x lower the acceptor. The vertical double-headed arrow indicates the donor's peak emission wavelength of 460 nm.

#### 3.4 Determination of the switching efficiency of PS1 (quantitative composition of the photostationary state)

The switching efficiency was determined by irradiating **PS1** for 10 min with a 310 nm LED in a 50  $\mu\text{L}$  cuvette with a concentration of 3  $\mu\text{M}$ . The sample was then analysed via an HPLC with a Synergi Fusion-RP (80  $\text{\AA}$ , 4  $\mu\text{m}$ , 150 x30 mm, Flowrate 1mL/min) to separate the two different isomers. The two diastereomers of the closed ring form also absorb light in the visible range and can therefore be differentiated from the open isomer. Integration of the corresponding peaks leads to the ratio between the open and the closed isomer. The extinction coefficients of both isomers at 260 nm are nearly the same due to the strong absorption of the nucleotides at this wavelength, which allows the integration of the peaks to extract the switching efficiency. For PS1, a switching efficiency of 50 % could be determined.

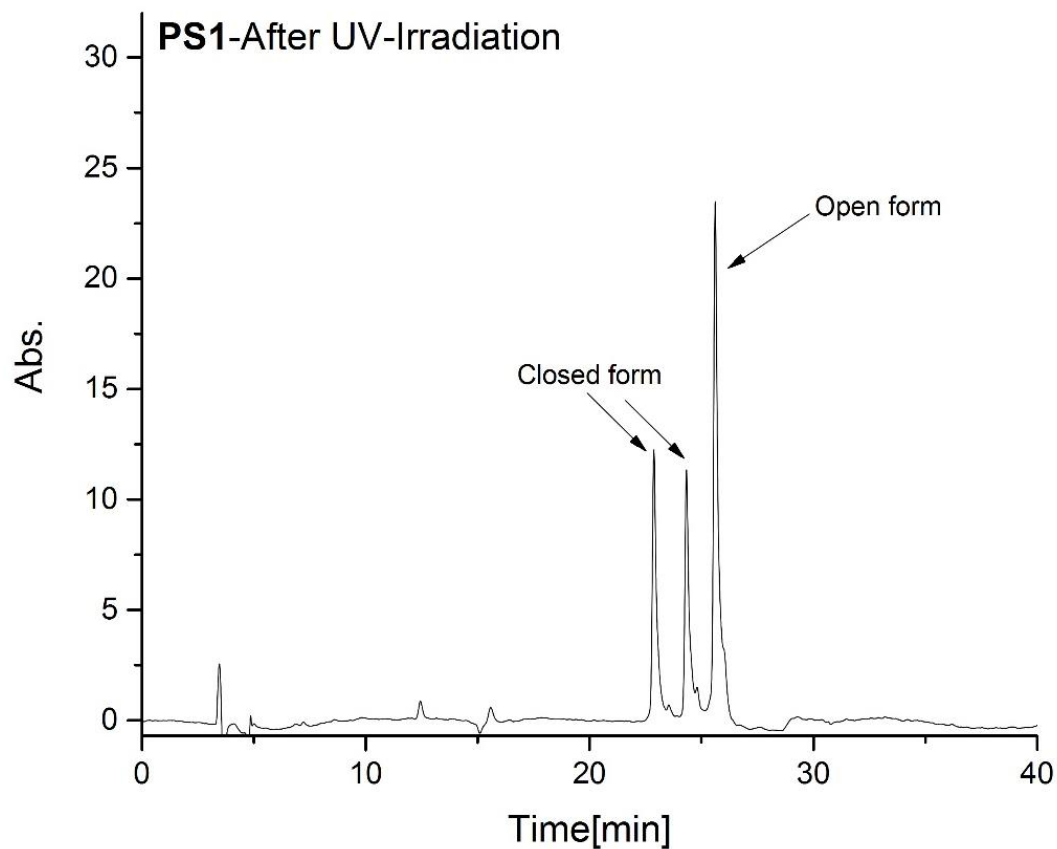


**Figure 3.2 HPLC time trace of PS1 after 10 min of UV-irradiation with a 310 nm LED (Thorlabs M310L3) at 260 nm.**

**Table 3.2 HPLC gradient for the determination of the switching efficiency of PS1**

<b>Method D</b>	
<b>Time [min]</b>	<b>Buffer B [%]</b>
0	7.5
10	12.5
35	40
40	50
45	100
50	100
52	7.5

### 3.5 Absorbance of one *versus* three photochromic nucleotides.

Photochromic strands PS1 and PS3 were hybridized with the donor and acceptor strands to generate the all-optical excitonic switch in two different configurations as shown in Figures 2.1a and 2.1b. The expectation was that incorporation of three photochromic nucleotides would produce a three-fold increase in the donor-acceptor emission modulation. Figure 3.2 shows the saw-tooth plots created from the emission data collected for 5  $\mu\text{M}$  (Panels a and c) and 20 $\mu\text{M}$  (Panels b and d) concentrations in the liquid environment with either one (Panels a and b) or three (Panels c and d) photochromic nucleotides attached. When a single photochromic nucleotide was used (Fig. 3.2a & 3.2b), the donor and acceptor emission was compared after each opening and closing event to reveal any saw-tooth behavior indicative of modulation. For the 5  $\mu\text{M}$  single photochromic nucleotide sample, modulation is initially barely visible (1.0% and 0.6%) but disappears during later cycling. However, for the 20  $\mu\text{M}$  sample, a 6.6% and 5.0% saw-tooth modulation is observed. When three photochromic nucleotides were present (Figs. 3.2c & 3.2d), clear modulation of the donor and acceptor emission were observed in the 5  $\mu\text{M}$  (8.2% and 7.8% respectively) and 20  $\mu\text{M}$  samples (15.1% and 8.4% respectively).

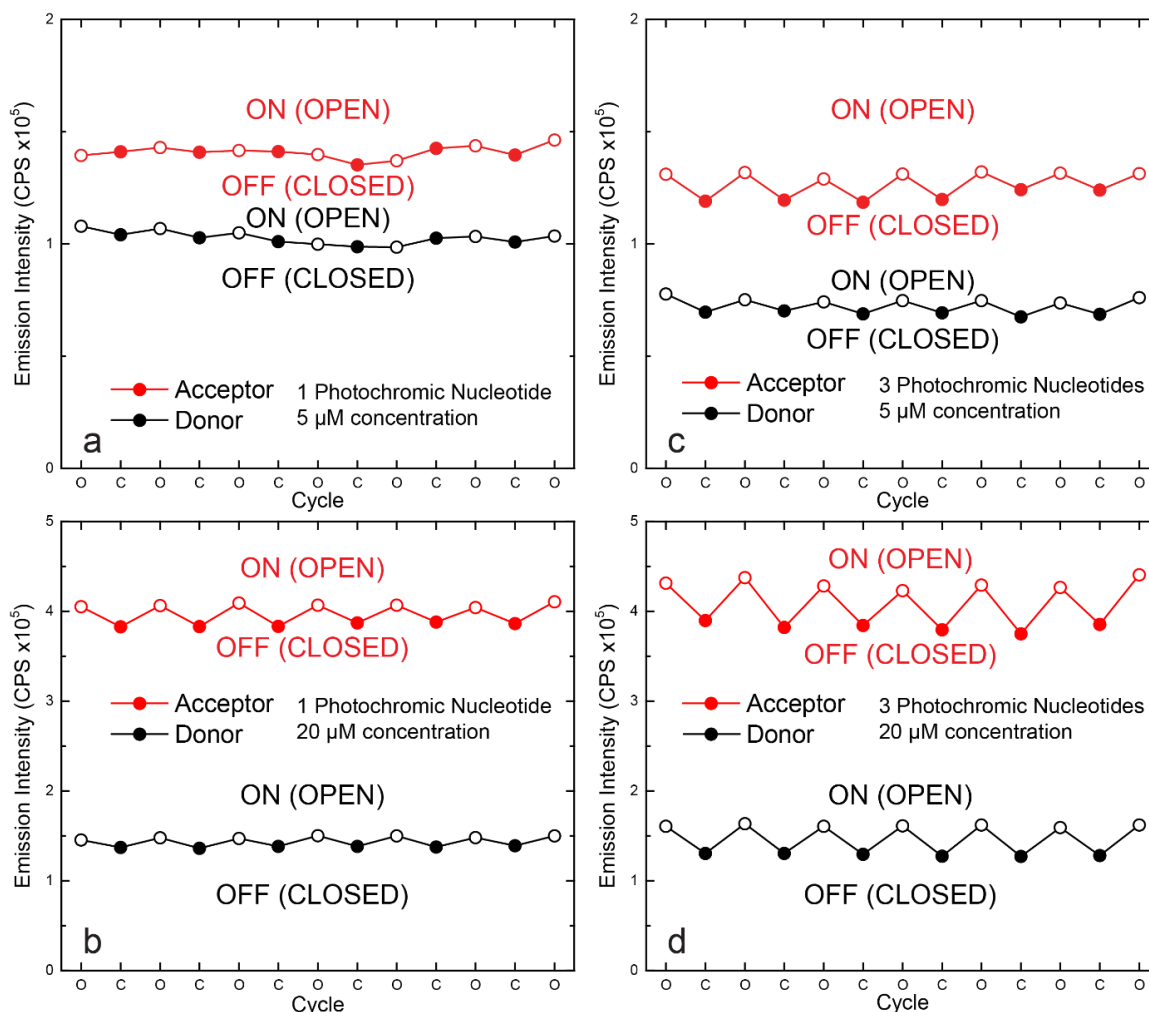


**Figure 3.2** Saw-tooth plots of the all-optical excitonic switch operating in the liquid phase demonstrating the changes in the donor and acceptor emission as the photochromic nucleotides are cycled between the open and closed configuration (i.e., ON and OFF states) six times. (a) 5 $\mu$ M switch with a single photochromic nucleotide (strand PS1) demonstrates minimal modulation between the ON and OFF states. (b) 20 $\mu$ M switch with a PS1 strand demonstrates 6.6% modulation between the ON and OFF state. The weak modulation noted in a may be due to the emission of the donor/acceptor pair overwhelming the single photochromic nucleotide as well as the low absorbance of the single photochromic nucleotide. (c) 5 $\mu$ M switch with three photochromic nucleotides attached (PS3 strand) demonstrates 8.2% modulation between the ON and OFF states. (d) 20 $\mu$ M switch with a PS3 strand produces the greatest amount of donor/acceptor emission modulation (15.1%). The increased modulation results from the greater absorbance provided by the three photochromic nucleotides.

### 3.6 Fluorescence measurements.

Optical characterization involving acquisition of both the absorbance and fluorescence spectra of the all-optical excitonic switch was performed. UV-Vis absorbance spectra were collected for each individual strand using a dual-beam Cary 5000 UV-Vis-NIR spectrophotometer (Agilent Technologies). Static and dynamic emission spectra were collected using a Fluorolog-3 spectrofluorometer (HORIBA Scientific). Fluorescence emission detector geometries are illustrated in Figure 3.3.

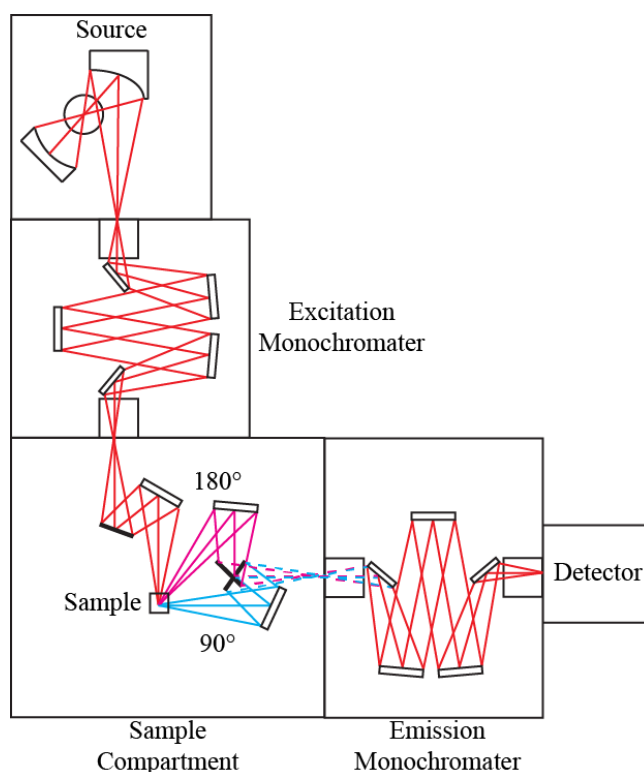


**Figure 3.3** Detector geometry for acquisition of all-optical excitonic emission spectra. For the liquid environment measurements, a perpendicular excitation light source interacts with the sample via a 2 mm by 2 mm window on the source side of the cuvette. The fluorescence emission is transmitted through a 2 mm by 10 mm window on the detector side of the cuvette (cyan lines) and detected via a photomultiplier tube (PMT, detector) aligned at  $90^\circ$  relative to the excitation. For the solid environment measurements, the excitation light source remained perpendicular to the sample, but the detector samples fluorescence emission aligned  $\sim 180^\circ$  relative to the sample (purple lines). The solid alignment geometry is required because very little fluorescence emission is delivered in the direction parallel to the quartz slide.

### 3.7 Controls.

In order to better understand the interaction of the photochromic nucleotides with the donor and acceptor chromophores, a series of control experiments were performed wherein specific DNA strands of the all-optical excitonic switch were replaced with bare ssDNA strands as illustrated in Figures 3.4a, 3.4d, 3.4g, and 3.4j. When the acceptor chromophore was omitted from the all-optical excitonic switch, (Fig. 3.4 a-c), we hypothesized that modulation of the donor by the photochromic nucleotides *via* absorption, FRET, or both processes should occur. As shown in Figure 3.1, the photochromic nucleotides in the closed absorbing configuration, (red dashed curve), can interact with both the donor absorbance (blue dashed curve) and emission (blue solid curve). Figures 3.4b & 3.4c demonstrate some emission intensity modulation, indicating the photochromic nucleotides absorb excitonic energy and interrupt FRET transfer of the donor emission. We therefore conclude the saw-tooth plot shown in Figure 3.4c validates our excitonic energy absorption hypothesis, which in turn causes FRET transfer modulation. Likewise, when the donor dye was omitted from the all-optical excitonic switch (Fig. 3.4 d-f), we hypothesized that the modulation of the acceptor by the photochromic nucleotides *via* absorption, FRET, or both should occur. As shown in Figure S1, the photochromic nucleotides in the closed absorbing configuration (red dashed curve) can interact with both the acceptor absorbance (green dashed curve) and emission (green solid curve). Figures 3.4e & 3.4f demonstrate some emission intensity modulation, confirming the hypothesis that the photochromic nucleotides also absorb excitonic energy and interrupt FRET transfer to the acceptor dye. We further hypothesized no modulation would be observed for the following controls: when photochromic nucleotides were not included in the switch

construct (Fig. 3.4g) or when both the donor and the acceptor were excluded from the switch construct (*i.e.*, only photochromic nucleotides present) and mixed in solution with a switch construct with only the donor and acceptor (*i.e.*, no photochromic nucleotide; Fig. 3.4j). For the latter control (Fig. 3.4j), we assumed that no near field interaction, and thus no modulation, would occur between the photochromic nucleotides-only switch construct and the donor/acceptor pair-only construct (Fig. 3.4j). Both negative controls, Figures 3.4 h-i & 3.4 k-l, demonstrate virtually no modulation took place when cycling the all-optical excitonic switch controls, thus substantiating our hypotheses. The data shown in Figure 3.4i do not show saw-tooth behavior and thus suggest that modulation *via* excitonic absorption or FRET interruption is not possible without the photochromic nucleotides present. Figure 3.4l does not show saw-tooth behavior and this absence of modulation reinforces the need for direct, distance dependent interaction of the photochromic nucleotides with the donor/acceptor pair in order to produce excitonic absorption and FRET interruption. We note the data shown in Figure 3.4k do indicate some inner filter effect<sup>1</sup> on the donor emission in the presence of the photochromic nucleotides-only switch; this can be seen by comparing the donor emission in Figure 3.4h and 3.4k. The control experiments do indicate there are a variety of potential pathways for energy transfer, and further studies, which are beyond the scope of this paper, are warranted and could be conducted in the future.



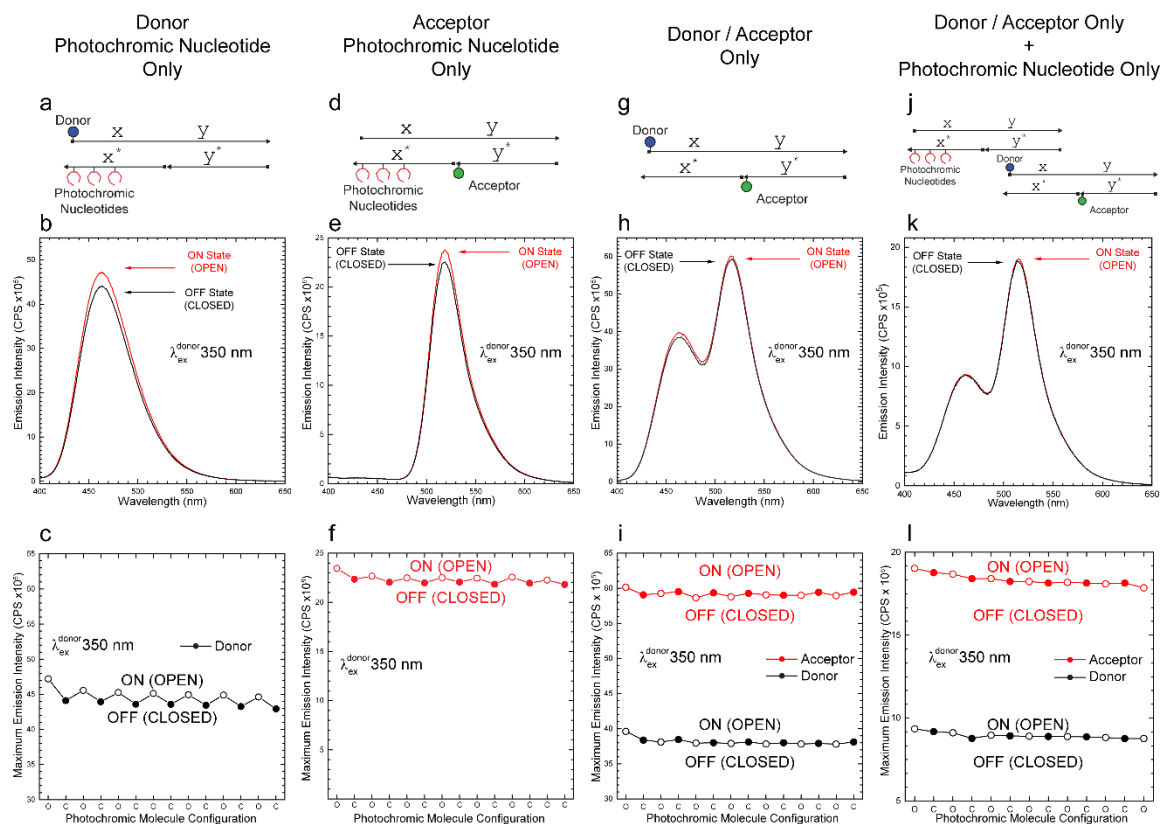


**Figure 3.4 All-optical excitonic switch controls performed at 5  $\mu$ M DNA concentration in the liquid environment. (a, b, c) Donor with three photochromic nucleotides hybridized (no acceptor present) produced slight modulation of the donor emission, indicating excitonic absorption and FRET transfer interruption. (d, e, f) Acceptor with three photochromic molecules hybridized (no donor present) produced slight acceptor emission modulation demonstrating excitonic absorption and FRET transfer interruption. (g, h, i) Donor/Acceptor with no photochromic nucleotides hybridized produced no significant modulation of either the donor or acceptor emission curve, signifying the excitonic absorption and FRET transfer interruption is directly attributable to the presence of the photochromic nucleotides. (j, k, l) Donor/Acceptor dyes hybridized plus three photochromic nucleotides hybridized to a bare all-excitonic construct outside the Förster radius produced negligible modulation. All data presented without normalization for concentration nor (in the case of k, l) for dilution.**

### 3.8 Solid phase concentration calculations

To determine the location of the all-optical excitonic switches in the solid phase sample, we collected a fluorescence optical image of the solid phase sample using a ProteinSimple FluoroChem Q MultiImage III chemiluminescent imaging system running AlphaView software version 3.4.0.0. as shown in Figure 3.5a. Since a 534 nm excitation

filter and a 606 nm emission filter was used, only the emission of the acceptor was collected. The grayscale image was reversed in order to enhance the contrast between the sample and the quartz slide, hence the emission is shown as black. The fluorescence image shows that the all-optical excitonic switches are located only in the outer elliptical ring of the solid phase sample.

To estimate the bulk concentration of the solid phase sample, profilometry measurements were performed using a Bruker Dektax XT-A Stylus profilometer (Fig. 3.5b). The profilometry data were plotted (Figs. 3.5c & d) and the resulting radial distances and profile height along the lateral and longitudinal ellipse directions were used to calculate the volume of the ellipse and, specifically, the volume of the outer elliptical ring. Note that most of the solid phase sample, and thus the all-optical excitonic switches, reside in the outer elliptical ring which correlates with the emission image (Fig. 3.5a) showing the location of the all-optical excitonic switches. The data suggest that evaporation while the sample was desiccated initially occurred from the center of the sample and moved outward during the transition from the liquid to solid phase. Hence, very little of the solid phase is within the inner ellipse and is instead primarily located in the outer elliptical ring. The solid phase concentration of all-optical excitonic switches can then be determined from the volume of the solid phase in the outer elliptical ring using the following Equations (1 – 6):

$$A_i = \pi r_1 r_2 \quad (1)$$

$$A_e = \pi r_3 r_4 \quad (2)$$

where  $r_1$  and  $r_2$  are the radii (major and minor) of the inner portion of the ellipse,  $r_3$  and  $r_4$  are the radii of the entire ellipse, and  $A_i$  and  $A_e$  are the areas of the inner and entire ellipses, respectively. The area,  $A_r$ , and volume,  $V_r$ , of the outer elliptical ring are given by:

$$A_r = A_e - A_t, \quad (3)$$

$$V_r = A_r H_r, \quad (4)$$

where  $H_r$  is the height of the outer elliptical ring. The concentration of the all-optical excitonic switches can be found using mass balance relationship:

$$C_r V_r = C_{liq} V_{liq}, \quad (5)$$

where  $C_r$  is the concentration of the all-optical excitonic switches in the outer elliptical ring while  $C_{liq}$  and  $V_{liq}$  are the concentration and volume of the liquid phase solution pipetted on the slide, respectively.

Solving for the concentration of the all-optical excitonic switches,  $C_r$ , we have:

$$C_r = \frac{C_{liq} V_{liq}}{V_r}. \quad (6)$$

Using the profilometry data, Equation 6 was used to calculate the concentration of the all-optical excitonic switches in the solid phase and is listed in Table 3.3.

As a frame of reference (*i.e.*, validity check) to  $C_r$  determined *via* Equation 6 using the profilometry data, a theoretical approach was also used to estimate the concentration of all-optical excitonic switches in the solid phase by using the volume of the double stranded DNA (dsDNA) scaffold,  $V_{dsDNA}$ , given by:

$$V_{dsDNA} = \pi r^2 l, \quad (7)$$

where the  $r$  and  $l$  are the radius and length of the dsDNA, respectively. The concentration of all-optical excitonic switches,  $C_{r,theory}$ , is determined by:

$$C_{r,theory} = \frac{1 \text{ switch mole}}{V_{dsDNA} \text{ Av \#}}, \quad (8)$$

where  $A_v \#$  is Avogadro's number. Equation 8 was used to calculate the theoretical concentration of all-optical excitonic switches in the solid phase and is listed in Table 3.3 to compare to that calculated by Equation 6. The comparison shows that the values are within an order of magnitude. Hence, the profilometry approach to determine the concentration of the all-optical excitonic switches in the solid phase is sound.

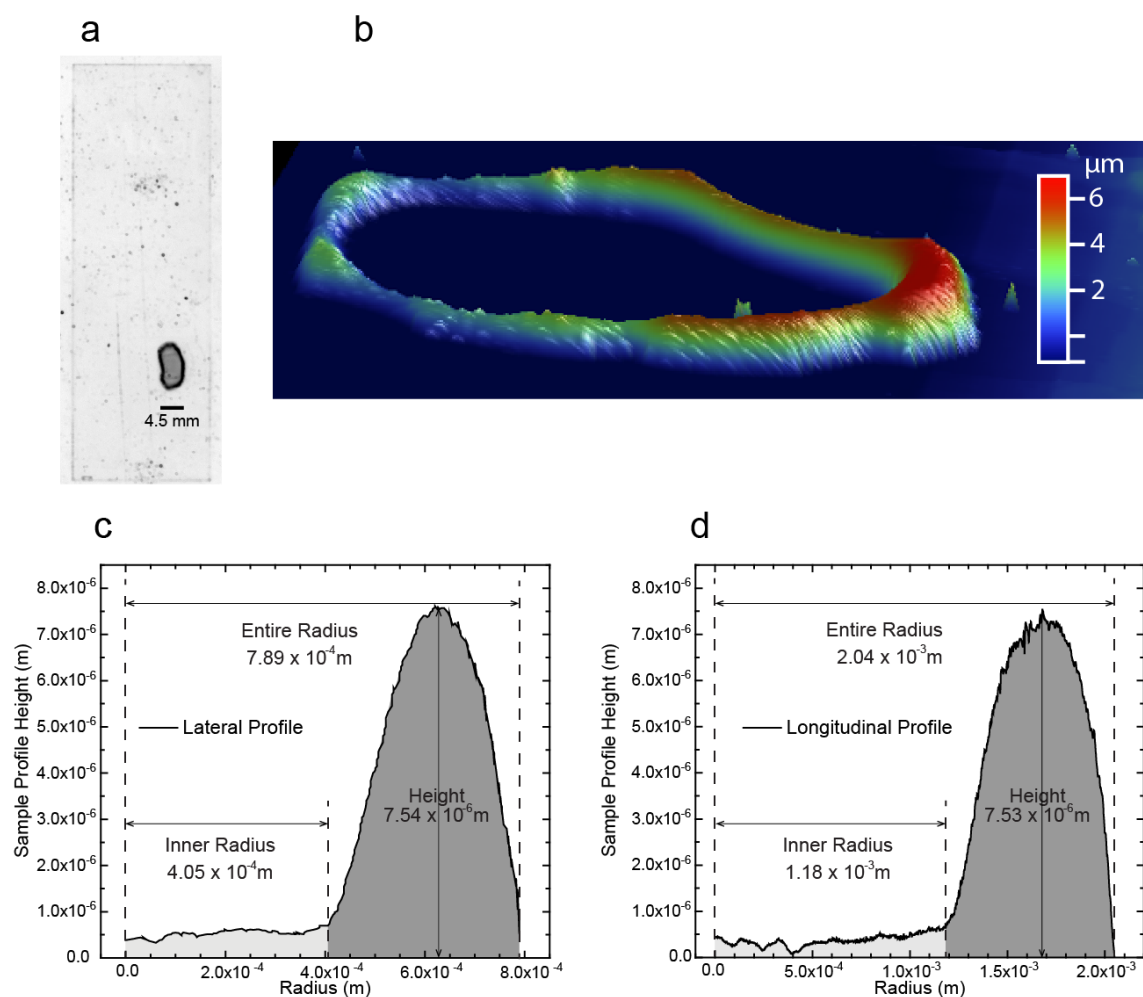


**Figure 3.5** (a) Representative solid phase sample imaged using a 534 nm excitation filter and a 606 nm emission filter; the grayscale image was reversed for clarity. A clear elliptical ring on the outer periphery can be observed in the image indicating the all-optical excitonic switch migrates to the edges of the sample during desiccation. The elliptical ring dimensions are confined within the window size of the fluorometer excitation beam. (b) 3D profilometer map of a representative solid phase sample where the elliptical ring is observed within the outer periphery of the sample. (c & d) Profilometer data collected from the solid phase sample along the lateral and longitudinal directions of the ellipse. For each direction, the sample height and the inner and outer ellipse radii are indicated. Note that the profiles have been divided into the non-fluorescing region (light shading) and the fluorescing region (dark shading).

**Table 3.3 Liquid and solid phase concentration values**

	Liquid Phase Volume, $V_{liq}$ (L)	Liquid Phase Concentration, $C_{liq}$ (M)	Solid Phase Volume, $V_r$ (L)	Solid Phase Concentration, $C_r$ (M)
Profilometer	$5.0 \times 10^{-6}$	$20 \times 10^{-6}$	$8.5 \times 10^{-9}$	$16 \times 10^{-3}$
Theoretical	X	X	X	$52 \times 10^{-3}$

### 3.9 Solid phase variation

A 30 nm blue shift is noted in the donor emission of the solid phase sample (Figure 2.2d). A potential cause of the blue shift in the solid phase sample may be due to solvatochromic changes of the chromophores as a result of solidification from the liquid phase.<sup>2</sup>

### 3.10 Switching time derivation:

Assuming a first order reaction rate for the all-optical switch's opening and closing upon exposure to specific wavelengths of light, the relationship between  $\Delta_s$  and  $t_e$  is:

$$\Delta_s = S \left[ \frac{(1 - e^{-t_e/\tau_o})(1 - e^{-t_e/\tau_c})}{1 - e^{-(\tau_o + \tau_c)t_e/\tau_o\tau_c}} \right], \quad (9)$$

where  $\tau_o$  and  $\tau_c$  are the mean time to modulate from closed to open, and the mean time to modulate from open to closed, respectively, and  $S$  is a single offset representative of the steady state equilibrium (see 3.11 for complete derivation). The simple elegance of Equation 9 allows  $\Delta_s$  versus  $t_e$  data to be modeled with a single parameter,  $S$ . The validity of the hypothesis is then tested by modeling  $\Delta_s$  versus  $t_e$  data using Equation 9.

Obtained from the static emission scans,  $\Delta_s$  of the donor or acceptor is defined as the fractional difference between the maximum emission intensities in the ON or OFF state of either the donor or the acceptor, and is given by:

$$\Delta_s = \frac{I_{open} - I_{close}}{I_{open}}, \quad (10)$$

where  $I_{open}$  and  $I_{closed}$  are the maximum donor (462 nm liquid and 433 nm solid) or acceptor (517 nm liquid and 513 solid) emission intensities when the photochromic nucleotides are in the open configuration or closed configuration, respectively. For each exposure time,  $\Delta_s$  was determined and plotted as a function of the state (ON *versus* OFF) as shown in Figure 2.3a.

Assuming first order reaction kinetics behavior for ring opening and closing of the photochromic nucleotides,<sup>3</sup> the dynamic modulation emission data (Figs. 2.2c & f) can be fit with an exponential function described by:

$$I = I_o e^{-t_e/\tau_i} + I_{offset}, \quad (11)$$

where  $I$ ,  $I_o$ ,  $t_e$ , and  $\tau_i$  are the final emission intensity of the donor or acceptor, the initial emission intensity of the donor or acceptor, the photochromic nucleotides' exposure time, and the mean time for modulation (time to open,  $\tau_i=\tau_o$ , or close,  $\tau_i=\tau_c$ , the photochromic nucleotides), respectively.  $I_{offset}$  establishes the donor or acceptor emission intensity offset from a zero baseline. From Equation 11, values for  $\tau_i$  may be extracted for both the closed to open cycle ( $\tau_o$ ) and open to closed cycle ( $\tau_c$ ), and their sum ( $\tau_{\Sigma}$ ) should theoretically be the same as  $t_s$ , the characteristic switching time shown below.

The data in Figure 2.2 of chapter 2 were obtained with a  $t_e$  of 30 seconds; therefore, only one  $t_e$  can be used in Equation 11. To determine the validity of our hypothesis (*i.e.*,

Equation 9), a set of time trial experiments were necessary and therefore performed over a range of specifically chosen  $t_e$ 's for the photochromic nucleotides and  $t_s$  was thereby obtained. For each  $t_e$  of the time trials experiments, saw-tooth plots were generated as shown in Figure 2.3a and 2.3d of chapter 2, and  $\Delta_s$  of the donor and the acceptor emission were calculated using Equation 10.

Equation 11 was used to fit the dynamic modulation data from each of the time trial experiments. Chapter 2 Figure 2.3b and 2.3e shows the fits of the averaged (6 data sets) dynamic modulation data for a photochromic nucleotide  $t_e$  of 30 seconds for both the liquid and solid phase, respectively. Both  $\tau_o$  and  $\tau_c$  were extracted from the liquid and the solid phase averaged dynamic modulation data. A  $\tau_o$  value of  $5.7 \pm 0.4$  (standard deviation) and  $11.8 \pm 5.1$  seconds was given for the liquid and solid phase, respectively, and a  $\tau_c$  value of  $8.4 \pm 0.5$  and  $8.1 \pm 2.8$  seconds was given for the liquid and solid phase, respectively (see Table 3.4 for all time trial data). The complete time to cycle between the open and closed state ( $\tau_{\Sigma}$ ) is  $14.1 \pm 0.9$  seconds for the liquid phase and  $19.9 \pm 7.8$  seconds for the solid phase. Figures 2.3b and 2.3e are representatives of all time trial dynamic modulation data collected.

### 3.11 Characteristic switching time derivation

#### 3.11.1 General equations

Here we obtain an expression for the switching amplitude as a function of time for the all-optical excitonic switch.

Let  $[O]$  denote the concentration of open photochromic nucleotides and let  $[C]$  denote the concentration of closed photochromic nucleotides, then:

$$[O] + [C] = [S], \quad (12)$$



where  $[S]$  is the total concentration of photochromic nucleotides.

Let  $I_o$  denote the photon flux of the light source used to open the photochromic nucleotides and let  $\sigma_o$  be the absorbance cross-sectional area for photochromic nucleotides opening. Then, the equation for the rate with which closed photochromic nucleotides are being lost from the sample due to conversion into open photochromic nucleotides is:

$$\frac{d[C]}{dt} = -\sigma_o I_o [C]. \quad (13)$$

Similarly, let  $I_c$  be the photon flux of the light source used to close the photochromic nucleotides and let  $\sigma_c$  be the absorbance cross-sectional area for photochromic nucleotides closing. The rate with which the open photochromic nucleotides are being removed from the sample by conversion into closed photochromic nucleotides is:

$$\frac{d[O]}{dt} = -\sigma_c I_c [O]. \quad (14)$$

It is useful to introduce the switching rates ( $\gamma_i$ ) and switching times ( $t_i$ ) for opening ( $i = o$ ) and closing ( $i = c$ ) the photochromic nucleotides according to:

$$\gamma_o = \frac{1}{t_o} = \sigma_o I_o, \quad (15)$$

and

$$\gamma_c = \frac{1}{t_c} = \sigma_c I_c. \quad (16)$$

### 3.11.2 Switching equations

We consider the case when the all-optical excitonic switch is being cycled back and forth between the open and closed configuration. Consider a sequence of exposure times  $t_n$  labeled by successive integers  $n$ , where  $n = 0, 1, 2, 3, \dots$ , at which cycling from one configuration to the other is initiated. During the times  $t$  for which  $t_{2n} < t < t_{2n+1}$  the

photochromic nucleotides are being exposed with light that opens the photochromic nucleotides. Hence, from Equations (13) and (15) one has:

$$\frac{d[C]}{dt} = -\gamma_o [C], \text{ when } t_{2n} < t < t_{2n+1}. \quad (17)$$

During the times  $t$  for which  $t_{2n+1} < t < t_{2n+2}$ , the photochromic nucleotides are being exposed with light that closes the photochromic nucleotides. Hence, from Equations (14) and (16), one obtains:

$$\frac{d[O]}{dt} = -\gamma_c [O], \text{ when } t_{2n+1} < t < t_{2n+2}. \quad (18)$$

Integrating Equation (17) within the exposure time interval  $t_{2n} < t < t_{2n+1}$  gives:

$$[C] = [C]_{t_{2n}} e^{-\gamma_o(t-t_{2n})}, \text{ for } t_{2n} < t < t_{2n+1}. \quad (19)$$

Integrating Equation (18) within the exposure time interval  $t_{2n+1} < t < t_{2n+2}$  gives:

$$[O] = [O]_{t_{2n+1}} e^{-\gamma_c(t-t_{2n+1})}, \text{ for } t_{2n+1} < t < t_{2n+2}. \quad (20)$$

Evaluating the concentrations at the end of the exposure time intervals, Equations (19) and (20) yield:

$$[C]_{t_{2n+1}} = [C]_{t_{2n}} e^{-\gamma_o(t_{2n+1}-t_{2n})}, \quad (21)$$

$$[O]_{t_{2n+2}} = [O]_{t_{2n+1}} e^{-\gamma_c(t_{2n+2}-t_{2n+1})}. \quad (22)$$

We now take all the exposure time intervals to be the same, that is:

$$t_{n+1} - t_n = t_e \text{ for all } n. \quad (23)$$

Hence, Equations (21) and (22) become:

$$[C]_{t_{2n+1}} = [C]_{t_{2n}} e^{-\gamma_o t_e}, \quad (24)$$

$$[O]_{t_{2n+2}} = [O]_{t_{2n+1}} e^{-\gamma_c t_e}. \quad (25)$$

Using Equation (12), this last equation yields:

$$[S] - [C]_{t_{2n+2}} = ([S] - [C]_{t_{2n+1}}) e^{-\gamma_c t_e}. \quad (26)$$

This can be rearranged to give:

$$[C]_{t_{2n+2}} = [S](1 - e^{-\gamma_c t_e}) + [C]_{t_{2n+1}} e^{-\gamma_c t_e}. \quad (27)$$

Using Equation (21) this becomes:

$$[C]_{t_{2n+2}} = [S](1 - e^{-\gamma_c t_e}) + [C]_{t_{2n}} e^{-(\gamma_o + \gamma_c) t_e}. \quad (28)$$

When cycling back and forth for over a long period of time, steady state is achieved in which:

$$[C]_{t_{2n+2}} = [C]_{t_n}, \text{ for all } n, \quad (29)$$

and similarly for the  $[O]$  concentration. Hence, Equation (28) becomes:

$$[C]_{t_{2n}} = [S](1 - e^{-\gamma_c t_e}) + [C]_{t_{2n}} e^{-(\gamma_o + \gamma_c) t_e}. \quad (30)$$

Solving this equation for  $[C]_{t_{2n}}$  yields the steady-state value:

$$[C]_{t_{2n}} = [S] \frac{1 - e^{-\gamma_c t_e}}{1 - e^{-(\gamma_o + \gamma_c) t_e}}. \quad (31)$$

Substituting Equation (31) into Equation (24) yields the following expression for the steady state value of  $[C]_{t_{2n+1}}$ :

$$[C]_{t_{2n+1}} = [S] \frac{e^{-\gamma_o t_e} (1 - e^{-\gamma_c t_e})}{1 - e^{-(\gamma_o + \gamma_c) t_e}}. \quad (32)$$

The switching amplitude  $\Delta_s$  is the difference, as measured by emission, between the concentration of closed photochromic nucleotides with respect to the former exposure time and the most recent exposure time given by:

$$\Delta_s = [C]_{t_{2n}} - [C]_{t_{2n+1}}. \quad (33)$$

Substituting Equations (31) and (32) into Equation (33) gives:

$$\Delta_s = [S] \frac{(1 - e^{-\gamma_o t_e})(1 - e^{-\gamma_c t_e})}{1 - e^{-(\gamma_o + \gamma_c) t_e}}. \quad (34)$$

In terms of the exposure times, Equation (34) can be written as

$$\Delta_s = [S] \frac{(1 - e^{-t_e/t_o})(1 - e^{-t_e/t_c})}{1 - e^{-(t_o + t_c)t_e/t_o t_c}}. \quad (35)$$

In the limit of very large exposure times,  $t_e$ ,  $\Delta_s$  no longer changes because it can be assumed that all photochromic nucleotides are either in the closed or open configuration.

Hence, can be written as:

$$\lim_{\Delta t \rightarrow \infty} \Delta_s = [S], \quad (36)$$

that is, if the exposure time is long enough, all the photochromic nucleotides are cycled from one configuration to the other. Taylor expanding Equation (34) for small  $t_e$ , one has, to linear order:

$$\Delta_s = \frac{\gamma_o \gamma_c}{\gamma_o + \gamma_c} [S] t_e, \quad (37)$$

or, substituting Equations (15) and (16), gives:

$$\Delta_s = \frac{1}{t_o + t_c} [S] t_e. \quad (38)$$

At the point in which the limit of long exposure times first holds, that is,  $\Delta_s$  first becomes constant (does not vary) and Equation (36) holds, then Equation (35) and Equation (36) must be equivalent hence:

$$\frac{1}{t_o + t_c} [S] t_e = [S]. \quad (39)$$

The particular  $t_e$  at which  $\Delta_s$  first becomes constant is defined as the characteristic switching time,  $t_s$ . Thus, Equation (39) should be written as:

$$\frac{1}{t_o + t_c} [S]_{t_s} = [S]. \quad (40)$$

In order for Equation (38) and Equation (36) to be equivalent,  $t_s$  and the sum of  $t_o$  and  $t_c$  (*i.e.*,  $\tau_\Sigma$ ) must be the same. That is:

$$t_s = \frac{\gamma_o + \gamma_c}{\gamma_o \gamma_c} = t_o + t_c = \tau_\Sigma. \quad (41)$$

The value of  $t_s$  can be determined from a plot of  $\Delta_s$  versus  $t_e$  data in the following approach. The point of intersection between a vertical line, drawn from the x-axis, and  $\Delta_s$  versus  $t_e$  data at the time at which  $\Delta_s$  first shows non-varying, or constant, behavior provides the value of  $t_s$ . This approach is shown in Figure 2.3c and 2.3f of chapter 2.

### 3.12 Time trial design

For the time trial experiments, the photochromic nucleotides were exposed for cycle times ( $t$ ) of 1 second, 3 seconds, 5 seconds, 10 seconds, 30 seconds, 100 seconds, 300 seconds, and 1000 seconds (Table 3.4). Each cycle of the time trial was performed as a series of four sequential excitation/emission scans whereby *i*) the all-optical excitonic switch was initially set to the ON state and a static emission scan (400 nm to 650 nm) was collected while exciting the donor of the all-optical excitonic switch with 350 nm VIS light, *ii*) the photochromic nucleotides were exposed to 300 nm UV light ( $\tau_c$ ) while simultaneously collecting donor emission (460 nm), *iii*) a static emission scan (400 nm to 650 nm) was collected while exciting the donor of the all-optical excitonic switch with 350 nm VIS light, and *iv*) the photochromic nucleotides were exposed to 455 nm VIS light ( $\tau_o$ )

while simultaneously collecting acceptor emission (520 nm). Note that fitting of very short time scales (1, 3, and 5 seconds) is questionable due to the difficulty of fitting segments too short to observe curvature.

**Table 3.4 Summed exposure times ( $\tau_{\Sigma}$ ) for time trial experiments conducted with the all-optical excitonic switch. One complete cycle ( $t_o + t_c$ ) is given as  $\tau_{\Sigma}$  and the average time of all values with the standard deviations are included.**

		5 sec	10 sec	30 sec	100 sec	300 sec	1000 sec	Averaged time (sec)	Standard Deviation
LIQUID 20 $\mu$ M	$t_o$	5.44	5.07	5.68	5.93	6.14	5.75	5.67	$\pm 0.37$
	$t_c$	7.49	8.01	8.84	8.62	8.77	8.46	8.37	$\pm 0.52$
	$\tau_{\Sigma}$	12.93	13.08	14.52	14.55	14.91	14.21	14.04	$\pm 0.83$
SOLID 69 mM	$t_o$	1.90	10.89	13.97	14.43	14.40	15.06	11.77	$\pm 5.06$
	$t_c$	2.84	7.44	9.47	9.49	9.67	9.96	8.14	$\pm 2.75$
	$\tau_{\Sigma}$	4.74	18.32	23.45	23.92	24.07	25.02	19.92	$\pm 7.81$

### 3.13 Absorbance cross section

The absorbance cross-section ( $\sigma$ ) of the all-optical excitonic switch may be calculated by using the photon flux ( $J$ ) determined in the previous section and the extracted mean times for modulation shown in Table 3.4 as follows. Let  $P$  denote the probability that a given photochromic nucleotide is switched. The time rate of change of  $P$  is given by:

$$\frac{dP}{dt} = \sigma J (1 - P). \quad (42)$$

The general solution to this differential equation is:

$$P = 1 - \exp^{-(\sigma J t)}. \quad (43)$$

Using the boundary conditions, the initial condition is  $P = 0$  at ( $t = 0$ ), and the final condition is  $P = 1$  at ( $t = \infty$ ). For the final condition, it is assumed that, if one waits long

enough, all the photochromic nucleotides will have switched. Let  $t_{(1/2)}$  denote the exposure time needed to cause half the photochromic nucleotides to cycle; at this time  $P = 1/2$ . Substituting these two quantities in Equation (43) and solving for  $\sigma$ , one has:

$$\sigma = \frac{\ln(2)}{Jt_{(1/2)}}. \quad (44)$$

### 3.14 Photon energy, photon fluence, and photon flux

Photon energy ( $E$ ) was calculated for the two wavelengths utilized to cycle the configuration of the photochromic nucleotide using:

$$E = \frac{hc}{\lambda}, \quad (45)$$

where  $h$  is Planck's constant,  $c$  is the speed of light, and  $\lambda$  is the wavelength of interest. For this work, 300 nm light was used to switch the photochromic nucleotide between the open (ON) to closed (OFF) configuration (**o-c**) and 455 nm light was used to switch the photochromic nucleotide between the closed (OFF) to open (ON) configuration (**c-o**). Using Equation 45, the photon energy at 300 nm (**o-c**) is  $6.62 \times 10^{-19}$  Joules and at 455 nm (**c-o**) is  $4.37 \times 10^{-19}$  Joules.

The number of photons per second (photon fluence) is calculated with:

$$H = \frac{W}{E}, \quad (46)$$

where  $H$  is the photon fluence,  $W$  is the measured power and  $E$  is photon energy at 300 nm or 455 nm respectively. Power data collected from the Fluorolog-3 spectrofluorometer using a LABMAX\_TOP (Coherent Inc.) power meter (Model 1104622) coupled to a silicon diode photodetector (PM 30) was found to be  $60 \times 10^{-6}$  W at 300 nm and  $150 \times 10^{-6}$  W at 455 nm. Using Equation 46 the photon fluence is  $9.1 \times 10^{13}$

photons/sec at 300 nm and  $3.4 \times 10^{14}$  photons/sec at 455 nm. The photon flux ( $J$ ) (photons per unit area per second) is calculated with:

$$J = \frac{W}{EA}, \quad (47)$$

where  $A$  is the spot size area. Using a spot size of  $\sim 4 \text{ mm}$ ,<sup>2</sup> Equation 47 yields a photon flux of  $2.3 \times 10^{19}$  photons/( $\text{m}^2 \cdot \text{s}$ ) at 300 nm and  $8.6 \times 10^{19}$  photons/( $\text{m}^2 \cdot \text{s}$ ) at 455 nm respectively.

### 3.15 Ultrafast laser switching

Assuming use of a typical UV-VIS optical parametric amplifier (OPA) pumped by a 1 kHz regenerative amplified ultrafast Ti:sapphire laser (outputting sub 100 fs pulses) we can calculate the photon flux using:

$$\frac{J}{\text{pulse}} = \frac{E\lambda}{hcA}, \quad (48)$$

where  $E$  is the energy per pulse,  $\lambda$  is the wavelength of light to cycle the photochromic nucleotide,  $h$  is Planck's constant,  $c$  is the speed of light, and  $A$  is the spot size. Assuming 10  $\mu\text{J}$ /pulse with a beam radius of 100  $\mu\text{m}$  at the focused spot size area, Equation 48 yields a photon flux per pulse of  $4.8 \times 10^{20}$  photons/ $\text{m}^2$  at 300 nm and  $7.3 \times 10^{20}$  photons/ $\text{m}^2$  at 455 nm.

In order to determine the possibility of ultrafast switching of the photochromic nucleotide, we compared the photon flux produced by the Fluorolog-3 (see 3.13) in 30 seconds (see Figure 2.3c & 2.3f of chapter 2) to the photon flux produced by a sub 100 fs pulse produced by a typical ultrafast laser system. Using Equation 47, the Horiba produces a photon flux of  $6.8 \times 10^{20}$  photons/ $\text{m}^2$  in 30 seconds at 300 nm, whereas Equation 48



yielded a photon flux of  $4.8 \times 10^{20}$  photons/m<sup>2</sup> per pulse. This indicates the photon flux due to a single pulse from a typical ultrafast laser system should be sufficient to cycle the all-optical excitonic switch in the picosecond regime, with switching times limited by the intrinsic switching time of the photoswitch molecules rather than the ultrafast laser pulse duration.

### 3.16 Comparison of the all-optical excitonic switch to a 14 nm node FinFET

Although a direct comparison of the size and speed of our all-optical excitonic switch to a state-of-the-art (SOTA) MOSFET is arguably not directly possible, a simple comparison provides some insight into physical parameters of interest. Here, the SOTA MOSFET used in the comparison is a bulk 14 nm technology node FinFET that appears to be used in Intel's 14 nm technology node computer processing units (CPUs)<sup>4</sup>, which includes Intel's cutting-edge Broadwell, Skylake, and Kaby Lake CPUs. While Intel uses a three-FinFET configuration in their 14 nm technology node, we will only compare one FinFET and neglect gate pitch for simplicity. With these assumptions, the FinFET parameters calculated here can be considered lower bounds. Parameters for the bulk 14 nm technology FinFET are shown in Table 3.5<sup>4-7</sup>.

Both the power and energy of the FinFET can be estimated using the simple relationship<sup>5,7</sup>,

$$P = C_{load} V_{dd}^2 f + I_{leak} V_{dd}, \quad (49)$$

$$E = P/f, \quad (50)$$

where  $P$ ,  $E$ ,  $C_{load}$ ,  $V_{dd}$ ,  $f$ , and  $I_{leak}$  denote power, energy, load capacitance, supply voltage, operation frequency, and leakage current of a transistor, respectively. If we assume

that  $I_{leak}$  is low (not necessarily the case, but this favors the FinFET in the comparison), we can ignore the  $I_{leak}V_{dd}$  term and Equation 49 becomes:

$$P = C_{load}V_{dd}^2f. \quad (51)$$

We can approximate the  $C_{load}$  as the capacitance,  $C_{inv}$ , when the finFET is in inversion:

$$\begin{aligned} C_{load} &\sim C_{inv} \\ &= \frac{L_g W_{fin} \epsilon_0 k_{ox}}{EOT + t_Q}, \end{aligned} \quad (52)$$

where  $L_g$ ,  $W_{fin}$ ,  $\epsilon_0$ ,  $k_{ox}$ ,  $EOT$ , and  $t_Q$  are the gate length, fin width, permittivity of free space, high-k dielectric constant (HfO<sub>2</sub>), effective oxide thickness and quantum mechanical inversion layer thickness<sup>8</sup>, respectively.  $EOT$  is given by:

$$EOT = t_{IL} + \frac{k_{IL}}{k_{HK}} t_{HK}. \quad (53)$$

where  $t_{IL}$ ,  $t_{HK}$ ,  $k_{IL}$ , and  $k_{HK}$  are the interfacial SiO<sub>2</sub> layer thickness, the interfacial SiO<sub>2</sub> layer relative dielectric constant, and the relative dielectric constant of the HfO<sub>2</sub>, respectively. Using Equation 51, we can write the energy as:

$$E = C_{load}V_{dd}^2. \quad (54)$$

For a FinFET, we can now calculate the values of  $C_{load}$ ,  $E$ , and the energy for a full cycle (*i.e.*,  $2E$ ), which we define as ON-OFF-ON (see next paragraph). The values used for these calculations are listed in Table 3.5.

**Table 3.5 Bulk Low Power 14 nm technology node FinFET parameters (after6)**

Gate Length ( $L_g$ ):	14 nm
Fin Width ( $W_{fin}$ ):	10 nm
Fin Height ( $H_F$ ):	100 nm
Field oxide Height ( $H_{FO}$ ):	300 nm
SiO <sub>2</sub> Interfacial Layer Relative Dielectric Constant	3.9
High-k Gate Oxide Thickness ( $t_{HK}$ ):	~1.25 – 2.2 nm (used 1.5 nm)
HfO <sub>2</sub> Relative Dielectric Constant ( $k_{HK}$ ):	25
Interfacial SiO <sub>2</sub> layer thickness ( $t_L$ )	~1 nm
Quantum Mechanical Inversion Layer Thickness	0.3-0.4 nm (used 0.4 nm)
Source or Drain Contact Pad Area Regions ( $A_{s,d}$ ):	$L_{s,d} \times L_{s,d} = 40 \times 40 \text{ nm}^2$
Source/Drain Contact Pad Area Regions -	15 nm
Distance from Source to Drain ( $SD_d$ ):	$L_g + 2 \times SD_g = 44 \text{ nm}$
Distance from End of Source to End of Drain	$SD_d + 2 \times L_{s,d} = 124 \text{ nm}$
FinFET Footprint ( $A_{FET}$ )	$L_{s,d} \times SD_{tot} = 496 \text{ nm}^2$
FinFET Volume ( $V_{FET}$ )	$A_{FET} \times H_F = 49,600 \text{ nm}^3$
Drain or power supply voltage ( $V_{dd}$ ):	~0.7 – 1.2 V (used 0.7V in
Simulated Ring Oscillator Initial Cycle time <sup>9</sup>	10s of ps
$C_{FinFET} \sim C_{inv}$ (Equation 52)	0.059 fF
Energy/Cycle (Equation 54)	58 aJ

Though this approach is simplistic, the minimum energy requirements for switching the all-optical excitonic switch can be estimated using Equation 45 (Supporting Information 3.14) and multiplying the resultant photon energy values by the number of photochromic nucleotides present. For our device construct with three diarylethenes per photochromic nucleotide strand, the energy required to switch from the ON state to the OFF state (*i.e.*, the open configuration to the closed configuration) is 1.98 aJ (*i.e.*, 3 times the 0.66 aJ energy of a single 300 nm photon). The energy required for the reverse process (*i.e.*, OFF to ON state or closed to open configuration) is less, 1.32 aJ, due to the lower

energy per photon of the 455 nm photons used. Thus, the total energy consumed in one full switching cycle (*i.e.*, ON-OFF-ON or OFF-ON-OFF) is 3.3 aJ. Full parameters for the all-optical excitonic switch are shown in Table 3.6. Times to open and close the diarylethene photochromic nucleotide are taken from references<sup>10, 11</sup>.

**Table 3.6 Parameters for All-Optical Excitonic Switch**

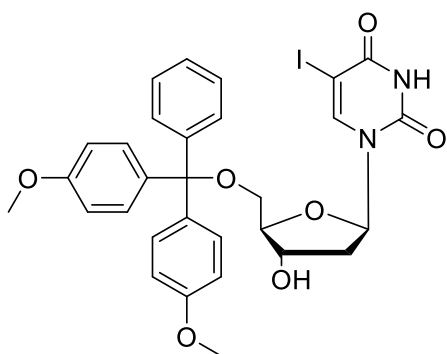
Length (L):	$\sim 20 \text{ bp} \times 0.34 \text{ nm} = 6.8 \text{ nm}$
Width (W):	2 nm
Height (H):	$2 \text{ nm} + 1 \text{ nm} = 3 \text{ nm}$
Footprint Area (A):	$L \times W = 13.6 \text{ nm}^2$
Volume (V):	$A \times H = 40.8 \text{ nm}^3$
Diarylethene decay time ( $t_d$ )	4 – 40 ps
Diarylethene open time ( $t_o$ )	40 ps
Diarylethene close time ( $t_c$ )	4 ps
Cycle time ( $t_c$ )	$t_o + t_c = 44 \text{ ps}$
Energy/Cycle	3.3 aJ

The energy to flip the FinFET to the ON state (*i.e.*, into strong inversion), using equation 54, was determined to be  $\sim 29$  aJ. The energy to flip the FinFET to the OFF state is assumed to be the same, hence the energy per cycle (*i.e.*, flipping from OFF to ON to OFF states) was calculated to be 58 aJ. Note that this energy/cycle is a lower bound since the energy due to the leakage current in the OFF state is ignored (see equations 49 and 50 and accompanying assumptions). Comparisons between similar parameters for the FinFET (Table 3.5) and the all-optical excitonic switch (Table 3.6) reveal that the all-optical switch's footprint is 37x more compact, volume is over 3 orders of magnitude smaller, and

energy consumption is over an order of magnitude less than that of the 14 nm FinFET. While it is difficult to find directly measured finFET cycle times, simulations show 14 nm FinFET ring oscillator initial cycle times in the 10s of ps and simulated write times to 6-finFET static random access memory (SRAM) in the 1s to 10s of ps, but do not discuss read times.<sup>9, 12</sup> It is reasonable to assume that cycle times for a single finFET is in the 10s of ps which is certainly comparable to or better than the photoisomerization reaction cycle times for diarylethene molecules. Although the calculations we have employed are simple first order approximations that one can argue should not be used as direct comparisons, they are rather compelling and do allude to the potential capabilities and impact of the all-optical excitonic switch for both low power and high speed applications relative to the current semiconductor electronics state of the art. Finally, in addition to the lower energy required per switching cycle for the all-optical excitonic switch calculated in the above comparison, it should be noted that the FinFET supply voltage,  $V_{dd}$ , is always applied, whereas once the all optical excitonic switch is in a given state (ON or OFF), the state is stable and thus no additional energy is required to maintain that state.

### 3.17 Photochromic nucleotide synthesis, attachment, and purification

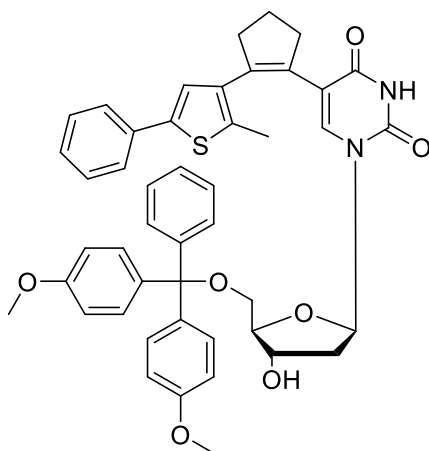
1-((2R,4S,5R)-5-((bis(4-methoxyphenyl)(phenyl)methoxy)methyl)-4-hydroxytetrahydrofuran-2-yl)-5-iodopyrimidine-2,4(1H,3H)-dione (**1**)



In a Schlenk flask under argon 5-iodo-2'-deoxyuridine (5 g, 14.12 mmol) was dissolved in dry pyridine (80 mL). 4,4-Dimethoxytritylchloride (DMT-Cl) (5.76 g, 17.01 mmol) was added and the mixture stirred overnight at room temperature. Ice water was added and the reaction mixture extracted with dichloromethane (DCM). The combined organic phases were washed with water and brine, dried over MgSO<sub>4</sub>, filtered, and the solvent removed under reduced pressure. Purification by flash column chromatography (silica gel, DCM/MeOH 50:1 + 1% NEt<sub>3</sub>) afforded **1** as a white solid with a yield of 85% (7.9 g, 12.0 mmol).

<sup>1</sup>H NMR (300 MHz, methanol-d<sub>4</sub>): δ = 8.20 (s, 1H), 7.51 – 7.18 (m, 9H), 6.93 – 6.83 (m, 4H), 6.23 (dd, J = 7.5, 6.0 Hz, 1H), 4.48 (dt, J = 5.8, 2.9 Hz, 1H), 4.05 (q, J = 3.2 Hz, 1H), 3.79 (s, 6H), 3.36 (d, J = 3.3 Hz, 2H), 2.46 – 2.27 (m, 2H).

1-((2R,4S,5R)-5-((bis(4-methoxyphenyl)(phenyl)methoxy)methyl)-4-hydroxytetrahydrofuran-2-yl)-5-(2-(2-methyl-5-phenylthiophen-3-yl)cyclopent-1-en-1-yl)pyrimidine-2,4(1H,3H)-dione (29) (2)



In a microwave vial **1** (100 mg, 0.15 mmol), 4,4,5,5-tetramethyl-2-(2-(2-methyl-5-phenylthiophen-3-yl)cyclopent-1-enyl)-1,3,2-dioxaborolane, (110 mg, 0.31 mmol), Pd(dppf)Cl<sub>2</sub> (7 mg, 8 μmol), and Cs<sub>2</sub>CO<sub>3</sub> (250 mg, 0.8 mmol) were dissolved in acetonitrile (2 mL) and water (1 mL) under argon.

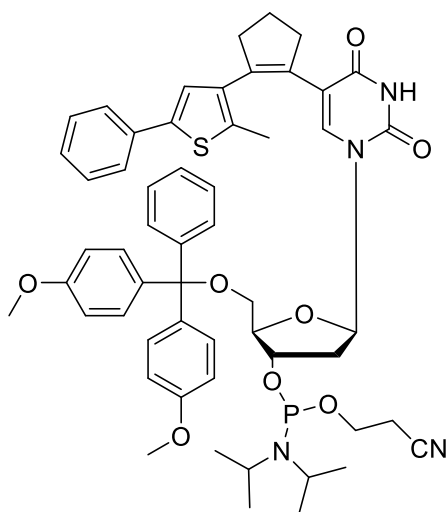
The mixture was degassed 3 times, the vial sealed, and stirred at 120°C for 1 hr. The reaction mixture was absorbed on silica and purified by flash column chromatography (silica gel, DCM/MeOH 20:1 + 1% NEt<sub>3</sub>), affording **2** as yellowish solid in a yield of 90% (104 mg, 0.13 mmol).

<sup>1</sup>H NMR (300 MHz, methanol-d<sub>4</sub>): δ = 7.60 – 7.18 (m, 14H), 7.11 (s, 1H), 6.88 – 6.77 (m, 4H), 6.70 (s, 1H), 6.18 (t, J = 6.6 Hz, 1H), 3.86 (dt, J = 7.4, 3.7 Hz, 1H), 3.80 (s, 3H), 3.75 (s, 3H), 3.63 (dt, J = 7.7, 4.0 Hz, 1H), 3.04 (ddd, J = 24.9, 10.2, 3.1 Hz, 2H), 2.84 (dt, J = 14.0, 7.2 Hz, 1H), 2.60 (dt, J = 14.8, 7.4 Hz, 2H), 2.16 – 2.08 (m, 1H), 2.07 (s, 3H), 2.05-2.00 (m, 1H), 1.57 (dt, J = 13.9, 7.1 Hz, 2H). <sup>13</sup>C NMR (125 MHz, methanol-d<sub>4</sub>): δ = 164.60, 160.15, 151.50, 146.24, 142.03, 138.94, 137.96, 137.30, 137.24, 136.74, 135.32, 134.58, 134.48, 133.37, 131.41, 131.21, 130.07, 129.34, 128.87, 128.43, 127.82, 126.28, 125.20, 114.21, 114.13, 113.14, 87.48, 87.16, 85.56, 75.83, 72.11, 65.70, 55.77,

41.49, 38.86, 25.03, 23.64, 14.12. HRMS (ESI, positive) m/z:  $[M+Na]^+$  calc. for  $[C_{46}H_{44}N_2O_7SNa]^+$ : 791.2761, found: 791.2725.



(2R,3R,5R)-2-((bis(4-methoxyphenyl)(phenyl)methoxy)methyl)-5-(5-(2-(2,5-dimethylthiophen-3-yl)cyclopent-1-en-1-yl)-2,4-dioxo-3,4-dihydropyrimidin-1(2H)-yl)tetrahydrofuran-3-yl(2-cyanoethyl) diisopropylphosphoramidite (**3**)



In a Schlenk flask under argon **2** (520 mg, 0.68 mmol) and Hünig's base (0.18 mL, 1 mmol) were dissolved in dry DCM (10 mL) and cooled down to 0°C. 2-cyanoethyl N,N-diisopropylchlorophosphoramidite (CEP-Cl, 0.31 mL, 1.1 mmol) was added, and the mixture was stirred at room temperature for 3 hrs. Purification via flash column chromatography (silica gel, DCM/MeOH 100:1 + 1% NEt<sub>3</sub>) afforded

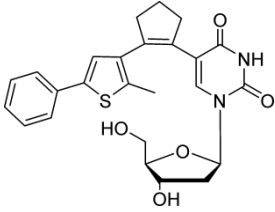
**3** as a white solid with a yield of 84% (550 mg, 0.57 mmol) as a mixture of isomers.

<sup>1</sup>H NMR (500 MHz, CDCl<sub>3</sub>): δ = 7.42 – 7.36 (m, 2H), 7.26 (s, 11H), 7.01 (d, J = 1.2 Hz, 1H), 6.79 (ddd, J = 8.8, 6.8, 2.0 Hz, 4H), 6.69 (d, J = 3.3 Hz, 1H), 6.18 (ddd, J = 7.8, 5.7, 1.9 Hz, 1H), 4.25 – 4.08 (m, 1H), 4.07 – 4.01 (m, 1H), 3.97 (tt, J = 6.8, 3.9 Hz, 1H), 3.95 – 3.84 (m, 2H), 3.79 (dd, J = 6.0, 4.7 Hz, 5H), 3.68 – 3.39 (m, 6H), 3.11 (dtd, J = 10.6, 6.5, 3.1 Hz, 2H), 3.01 (tt, J = 11.1, 5.6 Hz, 2H), 2.83 – 2.70 (m, 2H), 2.71 – 2.53 (m, 4H), 2.46 (t, J = 6.5 Hz, 1H), 2.30 – 2.18 (m, 2H), 2.08 – 2.01 (m, 4H), 1.50 – 1.41 (m, 1H), 1.38 (d, J = 13.8 Hz, 3H), 1.33 (t, J = 7.4 Hz, 1H), 1.29 – 1.21 (m, 8H), 1.20 – 1.14 (m, 4H), 1.11 (dd, J = 11.6, 6.8 Hz, 5H), 1.04 (d, J = 6.8 Hz, 3H), 0.92 (d, J = 6.8 Hz, 3H).

<sup>13</sup>C NMR (125 MHz, CDCl<sub>3</sub>): δ = 161.64, 158.76, 158.65, 149.50, 149.49, 144.61,

144.61, 140.73, 140.69, 137.49, 137.43, 137.11, 137.09, 136.23, 136.22, 135.50, 135.49, 134.20, 134.16, 133.63, 133.51, 133.00, 132.97, 130.45, 130.38, 130.08, 130.03, 129.08, 128.40, 128.34, 128.05, 128.04, 127.38, 127.36, 127.03, 126.99, 125.45, 125.39, 124.20, 124.14, 117.54, 117.46, 117.01, 113.31, 113.29, 112.43, 112.42, 110.16, 86.47, 86.46, 85.24, 85.21, 85.03, 84.98, 84.23, 84.20, 77.16, 73.78, 73.65, 73.46, 73.32, 64.11, 64.02, 64.01, 58.42, 58.40, 58.31, 58.27, 58.25, 55.42, 55.40, 55.37, 45.50, 45.45, 43.44, 43.36, 43.34, 43.26, 39.34, 38.13, 36.05, 36.03, 25.39, 25.37, 25.04, 25.03, 24.97, 24.72, 24.69, 24.66, 24.64, 24.59, 24.54, 24.53, 24.48, 23.15, 23.13, 23.06, 23.04, 22.80, 22.78, 20.43, 20.37, 20.30, 20.24, 20.17, 20.12, 14.17, 14.15. <sup>31</sup>P NMR (202 MHz, CDCl<sub>3</sub>): δ = 149.34, 148.94. HRMS (ESI, positive) m/z: [M+Na]<sup>+</sup> calc. for [C<sub>55</sub>H<sub>61</sub>N<sub>4</sub>O<sub>8</sub>SPNa]<sup>+</sup>: 991.3840, found: 991.3814.

**Table 3.7 Nucleotide modification.**

modified nucleoside	acronym	description
	<b>dU<sup>PS</sup></b>	Deoxyuridine-based photoswitchable nucleoside with phenyl substituent

**Table 3.8 Mass, sequence and chemical formula of the synthesized oligonucleotides.**

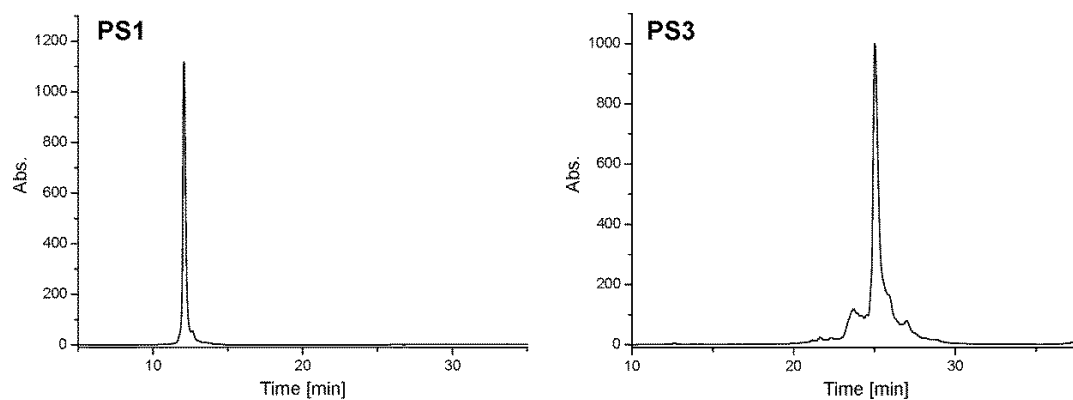
Name	Sequence	chemical formula	calculated mass [m/z]	found mass [m/z]
PS1	GGC TAG CTA CdU <sup>PS</sup> A CGA	C <sub>161</sub> H <sub>196</sub> N <sub>58</sub> O <sub>87</sub> P <sub>14</sub> S <sub>1</sub>	4800.8807	4800.8795
PS3	GGC TAG CdU <sup>PS</sup> A CdU <sup>PS</sup> A CdU <sup>PS</sup> A	C <sub>191</sub> H <sub>221</sub> N <sub>55</sub> O <sub>88</sub> P <sub>14</sub> S <sub>3</sub>	5224.0049	5223.9483

**Table 3.9 Gradients for preparative HPLC purification of the synthesized oligonucleotides**

Method A		Method B	
Time [min]	Buffer B [%]	Time [min]	Buffer B [%]
0	10	0	5
5	20	2	5
10	30	7	15
35	40	22	20
40	100	29	40
42	10	35	60
		45	100
		55	5

**Table 3.10 HPLC gradient for LC/MS measurements**

<b>Method C</b>	
Time [min]	Methanol [%]
0	10
5	20
10	30
35	40
40	100
42	10

**Figure 3.6 HPLC chromatograms of the synthesized oligonucleotides with one modification (PS1) and three modifications (PS3), detected at 280 nm.**

## References

1. Lakowicz, J. R., *Principles of Fluorescence Spectroscopy*, (1999). Kluwer Academic/Plenum Publishers, New York: 2004; pp 55-56.
2. Reichardt, C., Solvatochromic Dyes as Solvent Polarity Indicators. *Chem. Rev.* **1994**, *94*, 2319-2358.
3. Irie, M.; Fukaminato, T.; Matsuda, K.; Kobatake, S., Photochromism of Diarylethene Molecules and Crystals: Memories, Switches, and Actuators. *Chem. Rev.* **2014**, *114*, 12174-12277.
4. Lee, J.-H., Bulk FinFETs: Design at 14-nm Node and Key Characteristics. In *Nano Devices and Circuit Techniques for Low-Energy Applications and Energy Harvesting*, Springer: New York, 2016; pp 33-64.
5. Sugii, N., Low-Power Electron Devices. In *Green Computing with Emerging Memory*, Springer: 2013; pp 9-33.
6. Parikh, P.; Senowitz, C.; Lyons, D.; Martin, I.; Prosa, T. J.; DiBattista, M.; Devaraj, A.; Meng, Y. S., Three-Dimensional Nanoscale Mapping of State-of-the-Art Field-Effect Transistors (FinFETs). *Microsc. Microanal.* **2017**, *23*, 916-925.
7. Masuhara, T., The Future of Low-Power Electronics. In *Chips 2020*, Springer: New York, 2016; Vol. 2, pp 21-50.
8. Lubow, A.; Ismail-Beigi, S.; Ma, T. P., Comparison of Drive Currents in Metal-Oxide-Semiconductor Field-Effect Transistors Made of Si, Ge, GaAs, InGaAs, and InAs Channels. *Appl. Phys. Lett.* **2010**, *96*, 122105.
9. Sicard, E., Introducing 14-nm FinFET Technology in Microwind. Hyper Articles en Ligne (HAL), hal-01541171, **2017**, 25.
10. Shim, S.; Joo, T.; Bae, S. C.; Kim, K. S.; Kim, E., Ring Opening Dynamics of a Photochromic Diarylethene Derivative in Solution. *J. Phys. Chem. A* **2003**, *107*, 8106-8110.
11. Shim, S.; Eom, I.; Joo, T.; Kim, E.; Kim, K. S., Ring Closure Reaction Dynamics of Diarylethene Derivatives in Solution. *J. Phys. Chem. A* **2007**, *111*, 8910-8917.
12. Ansari, M.; Afzali-Kusha, H.; Ebrahimi, B.; Navabi, Z.; Afzali-Kusha, A.; Pedram, M., A near-Threshold 7T SRAM Cell with High Write and Read Margins and Low

Write Time for Sub-20 nm FinFET Technologies. *INTEGRATION, the VLSI journal* **2015**, 50, 91-106.

### CHAPTER THREE: SUMMARY AND FUTURE WORK

In conclusion, a scalable all-optical excitonic switch has been devised, assembled, and demonstrated in both the liquid and solid phases via DNA nanotechnology. This research encompassed design requirements for employing the programmability of DNA self-assembly to selectively organize and specifically control the number of optical components onto DNA-templated scaffolds. Employing diarylethene photochromic units for excitonic switching allowed successful operation through nearly 200 ON-OFF-ON cycles.

Listed below are the outcomes of the research toward realizing an all-optical excitonic switch included in this thesis (Chapter 2):

1. Design and construction of an all-optical excitonic switch for which resonant energy transfer was modulated solely by light with the capability of ultrafast switching times.
2. Collection of static and dynamic all-optical excitonic switch cycling (ON-OFF-ON) in both the liquid and solid phases.
3. Development of a model with only one fitting parameter to establish a characteristic switching time and switching amplitude in order to correlate static and dynamic all-optical excitonic switching.
4. Demonstration of no apparent cyclic fatigue of the all-optical excitonic switch by cycling 199 times to compare ON-OFF switching contrast.

5. Comparison of the all-optical excitonic switch to state-of-the-art MOSFET technology indicating a smaller footprint and lower energy per switch cycle power consumption.
6. Theoretical calculations indicating the all-optical excitonic switch can be operated in the picosecond regime with the use of a high peak power ultrafast laser.

This research offers encouraging results for the continued investigation into all-optical excitonic switching, specifically in the solid phase. A number of directions that may be explored for future studies include:

1. Development of diarylethene photochromic units possessing different absorption spectra to allow greater choices of optical components.
2. Increases in the number of diarylethene photochromic units employed in the all-optical excitonic switch to allow increased ON/OFF switching contrast.
3. Implementation of ultrafast laser switching to study high speed switching times in the picosecond regime and energy per cycle consumption in the attojoule range.